AD-782 630

MODEL TESTS OF AN ARCTIC SEV OVER MODEL ICE

E. J. Lecourt, et al

ARCTEC, Incorporated

Prepared for:

Office of Naval Research

1 August 1974

ARCTEC, Incorporated

Report 0062-9

i

MODEL TESTS
OF AN
ARCTIC SEV
OVER
MODEL ICE

BY

E. J. Lecourt
T. Kotras

1 August 1974

Sponsored By

Defense Advanced Research Projects Agency

D D C

AUG 5 1974

D

84
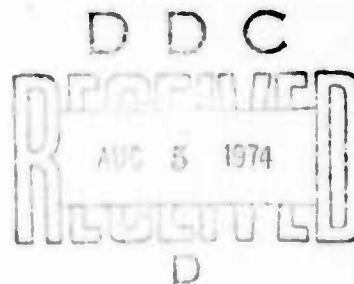
ARCTEC, Incorporated

i a

ACKNOWLEDGEMENT

DISCLAIMER

TABLE OF CONTENTS

NOMENCLATURE

Symbol	Definition
a	craft length
b	craft beam
C_1 C_2	bearing capacity coefficients
D	$Eh^3/12(1-\upsilon^2)$
F	friction force
E	Elastic Modulus
g	acceleration due to gravity
H	water depth
h	ice thickness
L	SEV cushion length
L_b	flat bottom length of hull
ℓ	characteristic length of the ice
N	normal force
P_1	load required to cause first crack
P_{max}	load required to cause complete breakthrough failure
p_0	water pressure on ice
R	ice resistance
t	time
u	craft velocity
u_c	critical velocity of flexural wave in ice
v	velocity

ARCTEC, Incorporated

vi

vi

Symbol	Definition
w	ice sheet deflection
x, y, z	coordinate system with z directed downward
Δ	weight of SEV
δ	Dirac delta function
λ	scale factor
μ	friction factor
υ	Poisson's Ratio (=.3)
ρ_i	mass density of ice
ρ_w	mass density of water
σ	ice flexural strength
ϕ	potential function
Δ^4	$\dfrac{\partial^4}{\partial x^4} + 2\dfrac{\partial^4}{\partial x^2 \partial y^2} + \dfrac{\partial^4}{\partial y^4}$

ARCTEC, Incorporated

- 1 -

I. SUMMARY

The model test program for the Arctic SEV consisted of two parts. The objective of the first part was to determine the resistance of an SEV operating over ice covered water. The second part of the test program was concerned with the problems associated with parking the Arctic SEV on the ice. Each part consisted of a series of model tests conducted in the ARCTEC Ice Model Basin, Savage, Maryland, to empirically determine the desired relationships between the independent and dependent test variables.

Resistance Tests

The hydrodynamic resistance of an SEV operating over calm water is primarily the wave-making resistance. The SEV traveling over water creates a train of waves moving at the speed of the craft. The energy expended by the SEV in generating these waves results in a drag force or wave resistance.

In a similar manner, when operating over a floating ice sheet, an SEV will generate a train of flexural waves in the ice sheet. The shape of these waves and, hence, the resistance of the SEV is a function of the mechanical properties of the ice sheet. The model tests demonstrated there is a peak resistance which occurs in the vicinity of the critical velocity of flexural waves in the ice sheet. The peaks, however, were found to be less than the primary hump in calm water and decrease with increasing ice thickness. Tables of data and a nondimensional analysis of the data is presented in Section III of this report.

ARCTEC, Incorporated

An unstable condition was observed with the model when operating near the critical velocity in thin ice. The shape of the wave generated in the ice sheet under the craft was such that it came in contact with the bow skirt. Friction between the skirt and the model ice caused the model SEV to pitch down by the bow until the hull made contact with the ice. This nose-in was observed only in the thinnest ice sheets of the tests; it was not experienced in the thicker ice sheets.

Notwithstanding the fact that the testing was performed with the model restrained in surge and that the skirt friction over the model ice is high, this phenomenon requires further investigation. It is, therefore, recommended that additional testing be performed specifically to investigate the interaction between the skirt system of the SEV with the wave generated in the ice sheet.

Parking Tests

The purpose of the parking tests was to determine the bearing capacity of the ice as a function of the size and shape of the landing pads and as a function of the thickness and properties of the ice. Five different landing pad configurations were tested in model ice sheets of various thicknesses and mechanical properties.

Analysis of the experimental data resulted in expressions for the bearing capacity for each model in the form of the following equations:

$$\frac{P_1}{\sigma_f h^2} = C_1 \left(\frac{L_b}{\ell}\right)^{1/2}$$

$$\frac{P_{max}}{\sigma_f h^2} = C_2 \left(\frac{L_b}{\ell}\right)^{1/2}$$

ARCTEC, Incorporated

- 3 -

where

P_1 = load required to cause the first crack to appear in the ice

P_{max} = load required to cause a complete breakthrough failure of the ice

h = ice thickness

σ_f = ice flexural strength

L_b = flat bottom length of SEV hull

ℓ = characteristic length of the ice

C_1, C_2 = constants determined experimentally and reported in Section IV.

Using these equations, the mode of failure of the ice during parking can be predicted as a function of the ice thickness. A summary of these predictions is presented in Table 8 of Section IV (reproduced on following page). From this table it is interesting to observe there is no tremendous difference between these landing pad configurations. Therefore in practical working terms the 170 ton craft will breakthrough the ice if the ice is less than about 1.5 feet.* On the other hand, the ice will support the craft without cracks forming if the ice is greater than approximately 2 feet.* Also, as noted in Section IV, these conditions can be improved significantly by increasing the size of the pad.

Because the ice did not support as much weight as was expected before the test, some of the above predictions are for ice thicknesses beyond the range of data collected during the model tests. It is, therefore recommended that additional tests be conducted in thicker ice in order to extend the range of the test data.

*
σ_f = 70 psi
E = 300,000 psi

ARCTEC, Incorporated

Table 8

Summary of Parking Test Results

Mode of Failure

	No Failure	Appearance of Cracks	Breakthrough Failure
170 ton ASEV			
with Four Inflated Pads	$h>2.2'$	$1.8'<h<2.2'$	$h<1.8'$
with Runners	$h>1.9'$	$1.5'<h<1.9'$	$h<1.5'$
with Rectangular Inflated Pad	$h>2.1'$	$1.3'<h<2.1'$	$h<1.3'$
540 ton ASEV			
with Four Inflated Pads	$h>3.7'$	$3.0'<h<3.7'$	$h<3.0'$
with Runners	$h>3.3'$	$2.6'<h<3.3'$	$h<2.6'$
with Rectangular Inflated Pad	$h>3.6'$	$2.3'<h<3.6'$	$h<2.3'$
1000 ton ASEV			
with Four Inflated Pads	$h>5.1'$	$4.2'<h<5.1'$	$h<4.2'$
with Runners	$h>4.5'$	$3.6'<h<4.5'$	$h<3.6'$
with Rectangular Inflated Pad	$h>4.9'$	$3.5'<h<4.9'$	$h<3.5'$

NOTE: Ice Flexural Strength (σ_f) = 70 psi
Ice Elastic Modulus (E) = 300,000 psi

ARCTEC, Incorporated

II. INTRODUCTION

The model test program for the Arctic Surface Effect Vehicle
(Arctic SEV) consisted of two parts. The objective of the first part was
to determine the resistance of an SEV operating over ice covered water.
The second part of the test program dealt with the problems associated
with parking the Arctic SEV on the ice. Each part consisted of a series
of model tests in the ARCTEC Ice Model Basin to empirically determine
the desired relationships between the independent and dependent test
variables.

The objective of the resistance tests was to determine the resistance
of an Arctic SEV as a function of its size, speed, thickness of ice, and
material properties of the ice. Particular emphasis was placed on deter-
mining the peak resistance at speeds near the critical velocity of flexural
waves in the floating ice sheets.

The objective of the parking tests was to determine the bearing
capacity of the ice as a function of the size and shape of the landing
pads and as a function of the thickness and properties of the ice.

Each part of the testing is discussed in separate sections of
this report.

III. RESISTANCE TESTS

Objective

The objective of the resistance tests was to determine the resistance of an Arctic SEV as a function of its size, speed, thickness of ice, and material properties of the ice. In addition, it was desired to study the dynamic behavior of the ice sheet to determine if the ice would interfere with the operation of the craft and if there was any possibility of broken ice damaging the hull structure.

Wave Resistance

The hydrodynamic resistance of an SEV operating over calm water is primarily the wave-making resistance. The SEV traveling over water creates a train of waves moving at the speed of the craft. The work done by the SEV in generating these waves results in a drag force or wave resistance. Recent theoretical investigations of wave resistance have been made by Newman and Poole [1], Barratt [2], and Doctors and Sharma [3].*

In a similar manner when operating over a floating ice sheet, an SEV will generate a train of flexural waves in the ice sheet. The shape of these waves and, hence, the resistance of the SEV will be influenced by the thickness of the ice and the mechanical properties of the ice sheet.

---

*Numbers in brackets designate references at end of paper.

Flexural Waves in a Floating Ice Sheet

An analysis of moving loads on a floating ice sheet has been performed by Nevel [4]. He uses the theory for the bending of thin plates to predict the deflection of the ice sheet, considering the ice to be homogeneous, isotropic, and elastic.

If a vertical, concentrated load P moves on the ice with a constant velocity u along the x-axis, the differential equation describing the motion of the plate is:

$$D\nabla^4 w + p_0 + \rho_i h \; \frac{\partial^2 w}{\partial t^2} = P \; \delta(x - ut)\delta(y) \qquad (1)$$

where

$D = Eh^3/12(1 - \nu^2)$

E = Young's modulus for ice

ν = Poisson's ratio for ice

h = ice thickness

$$\nabla^4 = \frac{\partial^4}{\partial x^4} + 2\frac{\partial^4}{\partial x^2 \partial y^2} + \frac{\partial^4}{\partial y^4}$$

x, y, z = a stationary cartesian coordinate system with z directed downward

w = the vertical deflection of the ice

p_0 = the water pressure on the ice

ρ_i = the mass density of the ice

ρ_w = mass density of water

t = time

u = velocity of the load

δ = Dirac's delta function

P = vertical, concentrated load

ARCTEC, Incorporated

From potential theory and assuming that the water is incompressible, the water pressure p_0 on the ice can be expressed as:

$$p_o = \rho_w g \omega - \rho_w \frac{\delta \phi}{\delta t}\bigg|_{z = \omega} \qquad (2)$$

where ϕ = scalar potential function. In this equation the non-linear velocity term has been neglected.

Nevel solved equation (1) and extended the solution to include the problem of a uniform, circular, pressure distribution of radius R by replacing P with

$$\int_0^R \int_0^{2\pi} (P/\pi R^2) \; r dr d\theta \qquad (3)$$

where P represents the total load.

The results of Nevel's work demonstrated that the ratio of the wave surface deflection to static deflection becomes infinite when the velocity u of the pressure distribution equals the critical velocity u_c, as illustrated in Figure 1. In addition, the critical velocity is found to be a function of the characteristic length of the ice sheet, density of water, density of ice, water depth and the size of the pressure distribution. In dimensionless terms, the relationship between critical velocity and these variables may be expressed as:

ARCTEC, Incorporated

FIGURE 1

DIMENSIONLESS ICE SHEET DEFLECTION

VERSUS

CRITICAL VELOCITY RATIO

$$\frac{\ell}{H} = 0 \qquad \frac{\rho_i h}{\rho_w \ell} = 0 \qquad \frac{R}{\ell} = 0$$

u/u_c = VELOCITY/CRITICAL VELOCITY

w/w_o = DEFLECTION/STATIC DEFLECTION

ARCTEC, Incorporated
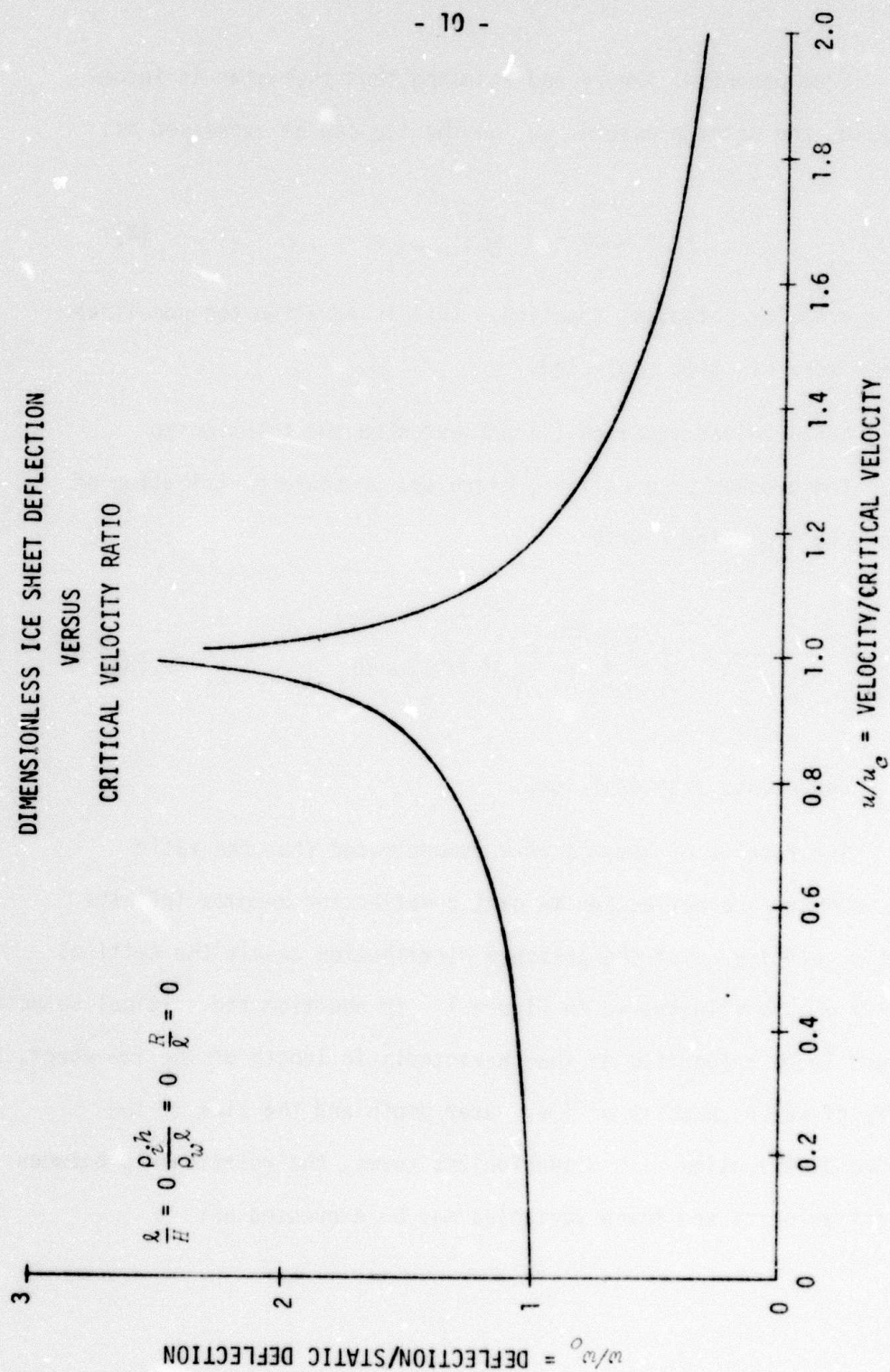
FIGURE 2

PLOT OF DIMENSIONLESS CRITICAL VELOCITY
VERSUS
DIMENSIONLESS DEPTH

$\dfrac{\rho_i h}{\rho_w \ell} = 0$

0.1

$\dfrac{u_c}{\sqrt{g\,\ell}}$

ℓ/H = CHARACTERISTIC LENGTH/WATER DEPTH

ARCTEC, Incorporated

- 12 -
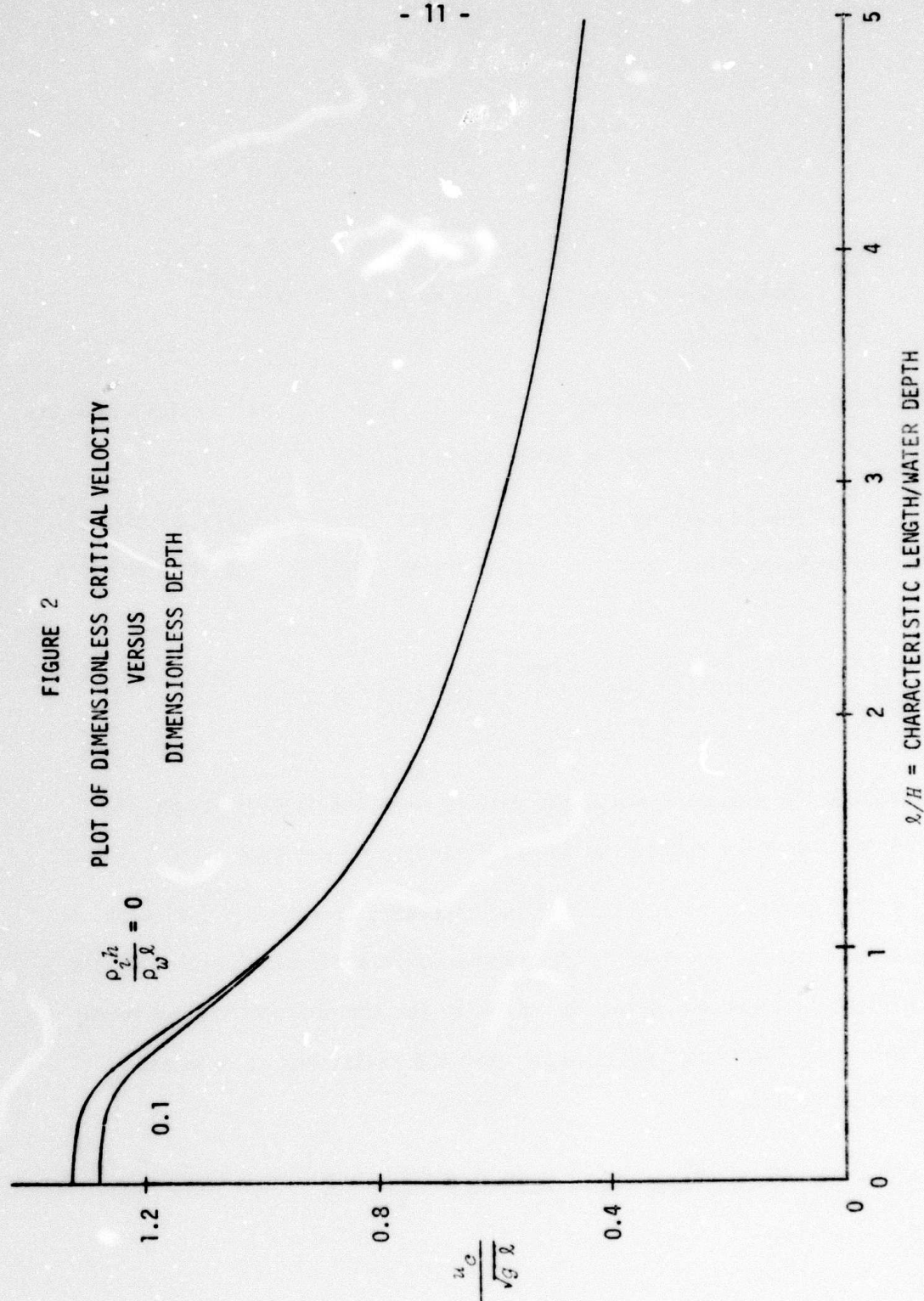
$$\frac{u_c}{\sqrt{g\ell}} = f_1\left(\frac{\ell}{H}, \frac{R}{\ell}, \frac{\rho_i h}{\rho_w \ell}\right) \tag{4}$$

where

ℓ = characteristic length of the ice sheet = $(D/\rho_w g)^{1/4}$

H = water depth

This relationship is presented in Figure 2. Note that the critical velocity is strongly dependent upon the depth of the water.

If the deflection of the ice is known, the resistance to motion experienced by the SEV can be estimated theoretically, using the following equation:

$$R_{ice} = \iint\limits_{S} p\,(x,y)\,\frac{dw}{dx}\,dx\,dy \tag{5}$$

where S is the area over which the uniform pressure is distributed and x is the Cartesian coordinate in the direction of motion.

For purposes of identifying the important independent variables, the case where the pressure is distributed over a circular area of radius R will be considered. Using the solution for the deflection from Nevel, the following functional relationship for the resistance is obtained from equation (5).

$$\frac{R_{ice}}{\Delta} = f_3\left(\frac{u}{u_c}, \frac{\ell}{H}, \frac{\rho_i h}{\rho_w \ell}, \frac{R}{\ell}\right) \tag{6}$$

where Δ is the weight of the model. The parameters contained in the function f_3 are all non-dimensional.

Two of the non-dimensional parameters contained in equation (6) can be neglected. For full-scale ice in deep water, the small variations in ℓ/H and in $\rho_i h/\rho_w \ell$ will have a very small influence on the resistance. For the model tests, ℓ/H varied from 0.093 to 0.234 and $\rho_i h/\rho_w \ell$ varied from 0.07 to 0.10. Nevel reports that variations in these parameters within the ranges indicated will have little influence on the critical velocity (Figure 2) and on the deflection (Figure 1). As a result, the critical velocity can be assumed equal to

$$u_c = 1.28 \ \sqrt{g\ell} \tag{7}$$

By eliminating these parameters from Equation (6) and converting this equation from polar coordinates to Cartesian coordinates, the following relation is obtained:

$$\frac{R_{ice}}{\Delta} \quad = \quad f_4 \left(\frac{u}{u_c} \ , \ \frac{b}{a} \ , \ \frac{a}{\ell} \right) \tag{8}$$

where a and b are the dimensions of the model. It should be noted that even though a and b are included as variables in Equation (8), they were constant for this test program since only one model was tested.

ARCTEC, Incorporated

Model Scaling Laws

For model testing to be correct, the model must be both geo-metrically similar and dynamically similar. The first is achieved by scaling all dimensions by λ, the geometric scale factor. The second condition is achieved by maintaining the ratio of significant forces the same for the model and full scale craft.

In testing an SEV over water, the significant forces are gravity forces and inertia forces. Gravity forces will scale by λ^3 since the density of water is the same for both the model and the full scale craft. It then follows that the inertia forces must also scale by λ^3. This is achieved by testing the model at velocities which correspond to the same Fronde Number (u^2/gL) as the full scale craft, where L is some charac-teristic dimension of the craft.

From these principles, the scaling laws listed in Table 1 can readily be derived. These laws dictate that the model ice thickness, flexural strength, and elastic modulus be reduced from the appropriate full scale values by the scale factor λ.

Table 1

Scaling Laws for Modeling

$h_{fs} = \lambda\ h_{ms}$ (h = ice thickness)

$\sigma_{fs} = \lambda\ \sigma_{ms}$ (σ = flexural ice strength)

$E_{fs} = \lambda\ E_{ms}$ (E = elastic modu'us)

$\rho_{wfs} = \rho_{wms}$ (ρ = mass density of water)

$\rho_{ifs} = \rho_{ims}$ (ρ = mass density of ice)

$t_{fs} = \sqrt{\lambda}\ t_{ms}$ (t = time)

$v_{fs} = \sqrt{\lambda}\ v_{ms}$ (v = velocity)

$R_{fs} = \lambda^3\ R_{ms}$ (R = resistance)

$I_{fs} = \lambda^5\ I_{ms}$ (I = mass moment of inertia)

$M_{fs} = \lambda^3\ M_{ms}$ (M = mass)

$\mu_{fs} = \mu_{ms}$ (μ = kinematic friction factor)

$B_{fs} = \lambda\ B_{ms}$ (B = beam)

$L_{fs} = \lambda\ L_{ms}$ (L = length)

$p_{fs} = \lambda\ p_{ms}$ (p = pressure)

The subscript fs is for full scale; and ms, for model scale. The symbol λ is the geometric scale factor (>1).

ARCTEC, Incorporated

Model SEV

The model used for the resistance tests was a 1/7.5 scale model of the SK-5 pictured in Figure 3. The characteristics of the model are:

Length Overall:	5.18 ft.
Beam:	3.17 ft.
Weight:	50.5 lbs.
Skirt Height:	0.47 ft.
Cushion Length:	4.06 ft.
Cushion Area:	9.78 ft.^{2}
Cushion Pressure:	5.16 psf
Fan Speed:	2800 rpm

The Arctic SEV Program is designing vehicles much larger than the SK-5; however, this model can be used without significant error to represent the larger craft by considering it to be of smaller scale. The appropriate scale factor is determined by the following relationship:

$$\lambda^3 = \frac{\text{weight of the full scale SEV}}{\text{weight of the model}}$$

Three sizes of SEV's are being considered. The nominal weights of these crafts are 170, 540, and 1000 short tons. For the SK-5 model to represent these crafts, the scale factors are those in Table 2. The cushion pressure of the model would then represent the full scale cushion pressures listed in the table.

For the resistance tests, the scale factor $\lambda = 19$ was chosen and the properties of the model ice were scaled appropriately.

Figure 3. Model of the SK - 5 (scale = 1/7.5)

ARCTEC, Incorporated

Table 2

Scale Factors Relating SK-5 Model
to Full Scale SEV

Full Scale Weight of SEV (Short Tons)	Scale Factor	Full Scale Cushion Pressure (psf)
170	19	97
540	28	140
1000	34	180

ARCTEC, Incorporated

Model Ice

The properties of the model ice must be scaled according to the scaling laws listed in Table 1 . The thickness h of the model ice, the flexural strength σ_f, and the modulus of elasticity E must be reduced from the full scale values by the scale factor λ, and the density ρ_i must be equal to the full scale value.

Control over these properties is possible using a synthetic model ice called MOD-ICE which has been developed by ARCTEC, Incorporated. This is a multi-component wax-like material which exhibits the desired properties. MOD-ICE was used for all of the resistance tests and will be referred to, herinafter, simply as "ice."

By controlling the properties of the model ice, dynamic similitude between the model and full scale vehicle is achieved.

Model Test Facilities

The ARCTEC Ice Model Basin in Savage, Maryland, is 60 feet long, 8 feet wide, and 4 feet deep. The water depth for the resistance tests was 2.9 feet.

Barratt [2] investigated the effect of water depth on wave resistance. His results show that a water depth equal to the craft length can be treated as deep water and that the wave resistance will increase approximately 3% at a water depth to craft length of 0.5.

ARCTEC, Incorporated

The ratio of water depth to craft length for the Arctic SEV tests was 0.72, indicating that the tank bottom would not significantly influence the resistance measurements.

With ice on the surface of the water, the effects of shallow water are related to the ratio of the characteristic length of the ice to the depth of the water. Nevel [4] determined this relationship, and his results have been included in Figure 2. From this information it has been concluded that the model tests were all conducted in deep water.

Newman and Poole [1] studied the effects of channel width on wave resistance. Their conclusions were that, except for the vicinity of $u^2/gH = 1$, the effects of the walls on the resistance are negligible for tank widths greater than two model lengths and not serious for widths greater than one model length. The ratio of the width of the tank to model length for these tests is 1.97.

The velocity corresponding to $u^2/gH = 1$ is 9.7 ft/sec or 5.7 knots. Near this velocity the resistance data in calm water and over ice was undoubtedly influenced by the tank walls.

The velocity in the towing basin was limited to less than 10 ft/sec primarily because of the length of the tank. At that velocity, the duration of the runs was only a few seconds, and higher speeds were not feasible. This limit was just above the primary hump.

Instrumentation

Instrumentation of the SEV model included the following:

- velocity
- resistance
- roll
- pitch
- heave
- cushion pressure
- ice sheet deflection

Each of the above variables was recorded on a light-pen oscil-lograph recorder.

The ice sheet deflection was measured using a linear variable differential transformer (LVDT). The LVDT was fixed to the tank wall about midway down the tank. The core of the LVDT rested on a small pad of stiff paper on the model ice. As the model flew past the LVDT, its core followed the rise and fall of the ice sheet. This signal was recorded on the oscillograph recorder and gave a time history of the flexural wave height in the ice at that location.

Ice Sheet Properties Measurements

As part of each test, the following properties of the ice sheet were routinely measured:

- thickness, h
- flexural strength, σ_f
- elastic modulus, E

ARCTEC, Incorporated

The ice thickness was measured every meter down the length of the tank. These were recorded and an average value calculated.

Flexural strength was measured by cutting several small cantilevers in the ice and measuring the forces required to break them. The strength was calculated using the following relationship:

$$\sigma_f = \frac{6Pl}{bh^2}$$

where P = force required to break the cantilever

l = length of the cantilever

b = breath of the cantilever

h = thickness of the cantilever

An average value was calculated for each model ice sheet. This is the method which has been used to measure ice strength during full scale tests in the Arctic. By performing the same test in the laboratory, the correct strength for model testing can be scaled from typical measurements made in the field.

The elastic modulus was measured by deflecting the ice sheet downward and measuring the force and the deflection at a distance r from the point of application of the force.

ARCTEC, Incorporated

Test Results and Analysis

The data collected during the resistnace tests are summarized in Table 3. The test data are also plotted in nondimensional form in the graph of Figure 4. The nondimensional resistance R/Δ is plotted versus the nondimensional velocity u/u_c with nondimensional characteristic length ℓ/L as a parameter.

Figure 4 shows that the wave resistance over ice has a peak which occurs at the critical velocity u_c of flexural waves in the ice sheet. This agrees with the theoretical prediction of Nevel [4] that the maximum wave amplitude, and hence the maximum resistance, would occur at the critical velocity.

The same data is plotted in Figure 5 as resistance R/Δ versus Froude number $u/\sqrt{gL}$. This figure also includes the curve of resistance in calm water measured in the ARCTEC model basin. Two observations can be made from this plot. First, the presence of the floating ice sheet effects the velocity at which the peak resistance occurs. This velocity, the critical velocity u_c, is a function of the properties of the ice sheet and is not determined by the characteristics of the craft as is the hump in calm water. The second observation is that the magnitude of the peak resistance is less than the calm water hump resistance.

In Tests 3, 5, 19, 20, and 21, the model pitched down by the bow and the hull made contact with the ice. This unstable behavior is similar to plow-in which has been experienced under certain conditions when

Table 3. Resistance Tests Data Summary

Test No.	Date	V (fps)	R* (lbs)	h (cm)	σ_f (kg/cm²)	ℓ (cm)	E (kg/cm²)	ω (in)	Pitch* (deg)	Roll* (deg)	Heave* (in)	$R_0(V=0)$ (lbs)
1	2/25	3.87	3.51	0.723	0.653	7.55	91.1	---	---	---	---	-0.40
2	2/27	4.91	3.56	0.798	0.473	6.95	48.8	0.44	-0.71	-0.23	-0.40	-0.81
3	2/28	6.10	2.30	0.875	----	8.76	93.3	---	---	---	---	---
4	2/15	5.92	2.65	0.777	0.477	10.62	287.	---	+2.31	0.00	-0.60	-1.10
5	3/18	5.60	2.40	0.845	0.552	13.39	564.	---	---	---	---	---
6	3/20	5.35	1.83	0.825	0.341	12.43	450.	1.37	+2.04	+0.23	-0.32	-0.65
7A	3/22	5.93	-0.28	2.62	0.163	30.68	522.	0.52	+0.44	0.00	-0.43	-2.21
7B	→	6.84	1.63	→	→	→	→	1.47	+2.66	0.00	-0.46	-1.47
7C	→	7.82	2.09	→	→	→	→	1.54	+2.75	+0.31	-0.65	-1.44
7D	→	8.75	1.95	→	→	→	→	1.39	+3.15	-0.15	+0.11	-1.43
7E**	→	6.31	1.86	→	---	---	---	1.18	+2.49	-0.15	-0.43	-1.46
7F**	→	7.41	3.22	→	---	---	---	1.83	+3.06	-0.23	-0.36	-1.39
8A	3/26	5.90	3.16	1.72	0.183	20.62	378.	1.40	+0.98	+0.46	-0.78	-1.26
8B**	→	5.93	3.82	→	---	---	---	1.84	+0.04	-0.07	-0.79	-1.33
9	3/27	4.86	0.14	1.62	0.230	18.5	321.	0.24	0.00	0.00	-4.32	-1.30
10A	3/28	6.81	1.74	1.62	0.369	24.97	969.	1.39	+2.97	0.00	-0.11	-1.36
10B	→	6.35	2.10	→	→	→	→	1.60	+2.84	0.00	-0.19	-1.34
10C**	→	2.96	-0.91	→	---	---	---	---	0.00	0.00	-0.05	-1.27
11	4/1	5.37	0.64	1.76	0.221	21.49	414.	0.28	+0.27	0.00	-0.13	-1.32
12A	4/2	6.18	2.20	1.37	0.281	16.26	288.	1.77	+2.53	0.00	-0.24	-0.57
13A	4/3	5.26	1.39	0.98	0.322	14.26	466.	0.56	0.00	0.00	-0.41	---
19	4/24	≈5	---	1.20	0.132	14.90	304.	---	---	---	---	---
20	4/25	≈5	---	1.13	0.195	16.71	631.	---	---	---	---	---
21	4/26	≈5	---	1.38	0.175	15.60	192.	---	---	---	---	---

* Sign convention: R and R_0: positive is resistance; negative is thrust.
                 Pitch: positive is bow up.
                 Roll: positive is roll to starboard.
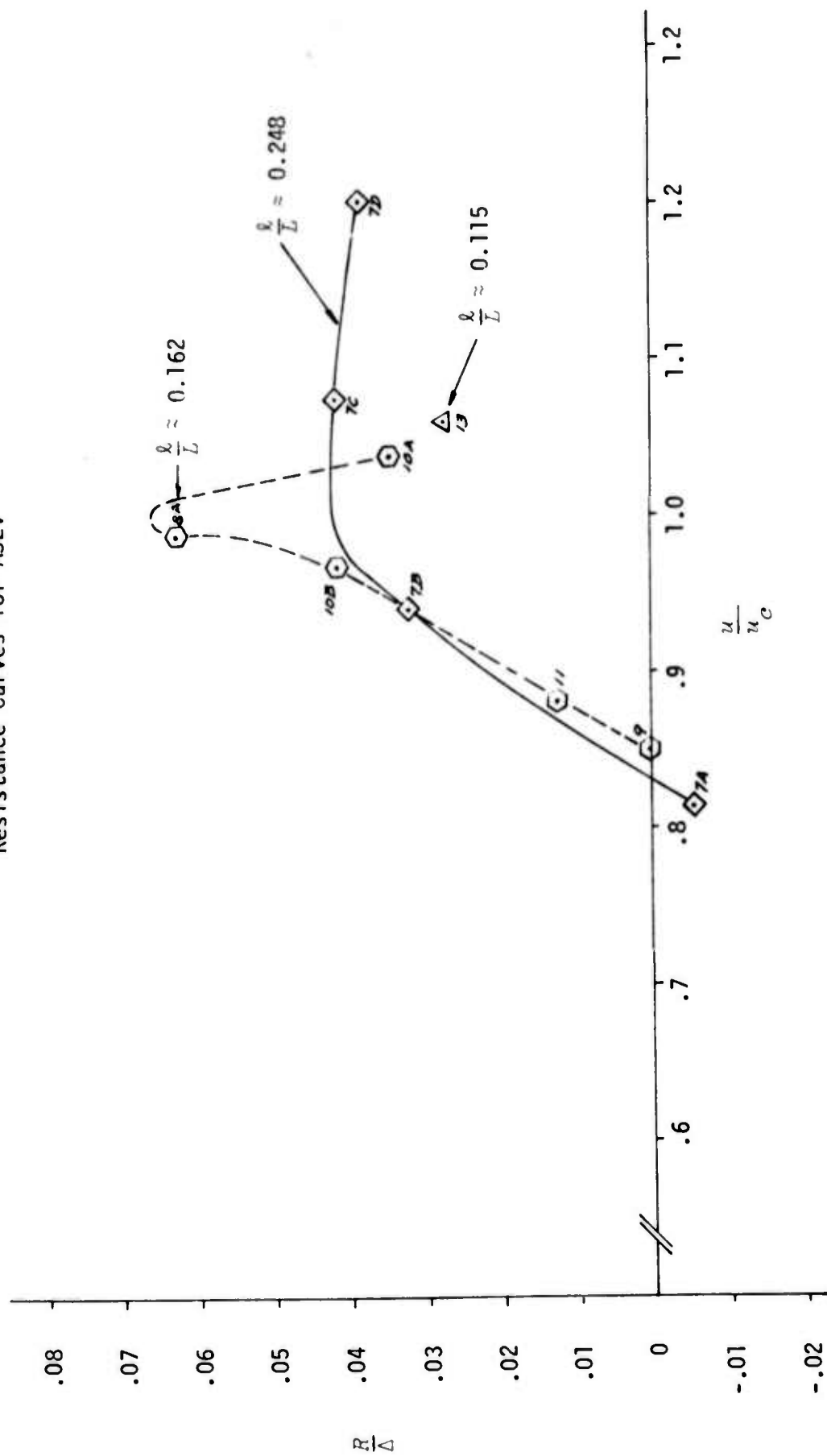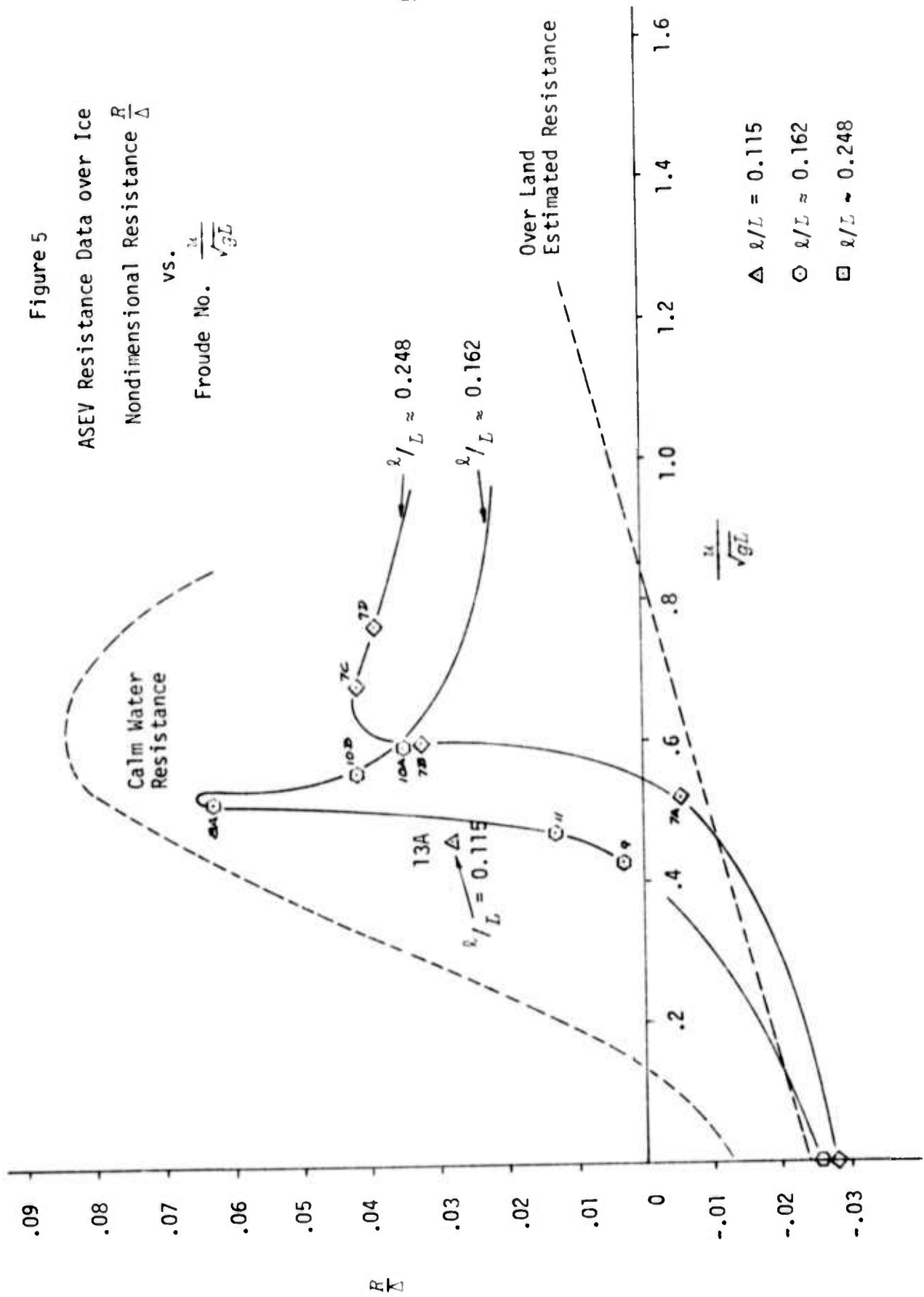   Heave: positive is up.

**Flying over broken ice sheet.

Table 3. Resistance Tests Data Summary (continued)

Test No.	u_c cm/sec	u/u_c	ℓ/L *	R/Δ	$\dfrac{u}{\sqrt{gL}}$	Remarks
1	110.1	1.071	0.061	0.0695	0.3384	
2	105.6	1.417	0.056	0.0685	0.4293	
3	118.6	1.568	0.071	0.0455	0.5333	Nose-in occurred
4	130.6	1.382	0.086	0.0525	0.5176	
5	146.6	1.159	0.108	0.0475	0.4896	Nose-in occurred
6	141.3	1.154	0.100	0.0363	0.4678	CG shifted aft
7A	222.0	0.814	0.248	-0.0055	0.5185	
7B		0.939	→	0.0323	0.5980	
7C		1.074		0.0414	0.6837	
7D		1.201		0.0386	0.7650	
7E	-----	-----	-----	0.0368	0.5517	
7F	-----	-----	-----	0.0638	0.6479	
8A	182.0	0.988	0.167	0.0627	0.5159	
8B	-----	-----	-----	0.0757	0.5185	
9	174.4	0.849	0.153	0.0028	0.4249	
10A	200.3	1.037	0.202	0.0345	0.5954	
10B	→	0.967	→	0.0416	0.5552	
10C	-----	-----	-----	-0.0180	0.2588	
11	185.8	0.881	0.174	0.0127	0.4695	CG shifted aft
12A	161.6	1.166	0.131	0.0436	0.5403	
13A	151.3	1.059	0.115	0.0275	0.4599	
19	154.8	1.016	0.120	-----	0.437	Nose-in occurred
20	163.9	0.929	0.135	-----	0.437	Nose-in occurred
21	158.4	1.039	0.126	-----	0.437	Nose-in occurred

* L = 123.8 cm

Figure 4

Resistance Curves for ASEV

Figure 5

ASEV Resistance Data over Ice

Nondimensional Resistance $\frac{R}{\Delta}$

vs.

Froude No. $\frac{u}{\sqrt{gL}}$

ARCTEC, Incorporated

operating SEV's over water. The bow skirt was tucked under the craft, and the resistance increased to a very high value. The ice thicknesses in which this occurred ranged from 0.72 to 1.2 cm, corresponding to 5.4 to 8.9 inches for the 170 ton craft. In each case, the craft was being flown at a speed near the critical velocity.

This nose-in, which occurred only in thin ice, is attributed to the interaction between the skirt and the ice caused by the shape of the flexural wave in the ice beneath the craft. This occurred a sufficient number of times to rule out an accidental cause. In considering this interaction the following factors should be noted:

(1) The model was towed at constant velocity and was not free to surge. The full scale SEV will be free to surge and will slow down as added resistance is met.

(2) The skirt of the model is not geometrically scaled for the 170 ton Arctic SEV.

(3) The location of the center of gravity and the flying trim of the full scale craft can be changed by the pilot.

(4) The skirt friction between the skirt and the model ice is greater than that with ice.

The model was successfully flown in thin ice near the critical velocity when the center of gravity was shifted aft 1.75% of the cusion length (0.0175 x 48.75 = 0.85 in.). In this condition, the nose-in problem was not experienced. The data from these tests were reported in Table 3 for Test No. 6, 12A, and 12B.

As part of the investigation of the nose-in problem, calm
water tests were conducted to evaluate the flying trim of the model;
and skirt friction tests were performed to determine the extent to which
friction contributed to the problem. The results of these tests are
reported in the following sections.

Calm Water Tests

Calm water tests were performed primarily to determine if the center
of gravity of the model SEV was correctly located. The results of these
tests are presented in Table 4 and in the graph of Figure 6 . Resistance
data from tests at NSRDC, Carderock, Maryland (Reference 5) are also
plotted in Figure 6 for comparison.

The resistance of the model measured in the ARCTEC Model Basin is
higher than that measured by NSRDC. This is attributed to the tank wall
effect which was discussed in an earlier section. The wall effect also
influenced the resistance measurements in model ice; however, since the
resistance data over ice has been compared to the calm water resistance
measured in the same test basin, the observations made and the conclusions
drawn are valid.

From these calm water tests, it was determined that the model weight,
location of the center of gravity, fan speed were correct and that the
model flew over water without any abnormal behavior. Except for the tests
where the CG was shifted aft for experimental purposes, these conditions
were set and held fixed for all tests.

Table 4

Calm Water Data

Δ = 50.5 lbs.
L = 4.06 ft.

Test No.	Date	V (kts.)	u (ft./sec.)	R (lbs.)	Pitch* (deg.)	Roll** (deg.)	R/Δ	$\dfrac{u}{\sqrt{gL}}$
1	3/5/74	1.25	2.12	0.042	+0.40	0.00	.0008	0.185
2	"	2.32	3.90	2.25	+2.35	-0.46	.0446	0.341
3	"	3.53	5.96	2.67	+2.53	-0.31	.0529	0.521
4	"	4.65	7.85	3.95	+4.48	-0.23	.0782	0.686
5	"	5.79	9.78	3.08	+3.37	-0.39	.0610	0.855
6	"	4.62	7.80	3.78	+4.40	-0.23	.0749	0.682
1	4/23/74	1.76	2.97	1.35	-	-	.0267	0.260
2	"	2.88	4.86	2.66	-0.09	-	.0527	0.425
3	"	4.06	6.86	4.47	+4.22	-	.0885	0.600
4	"	4.63	7.82	4.31	+3.86	-	.0853	0.684
5	"	5.27	8.89	4.03	+3.37	-	0798	0.777
6	"	3.55	6.00	3.40	+2.53	-	.0673	0.525
7	"	2.32	3.92	3.12	+2.26	-	.0618	0.343
8	"	1.15	1.94	0.703	+0.44	-	.0139	0.170

* For pitch, positive indicates bow up.
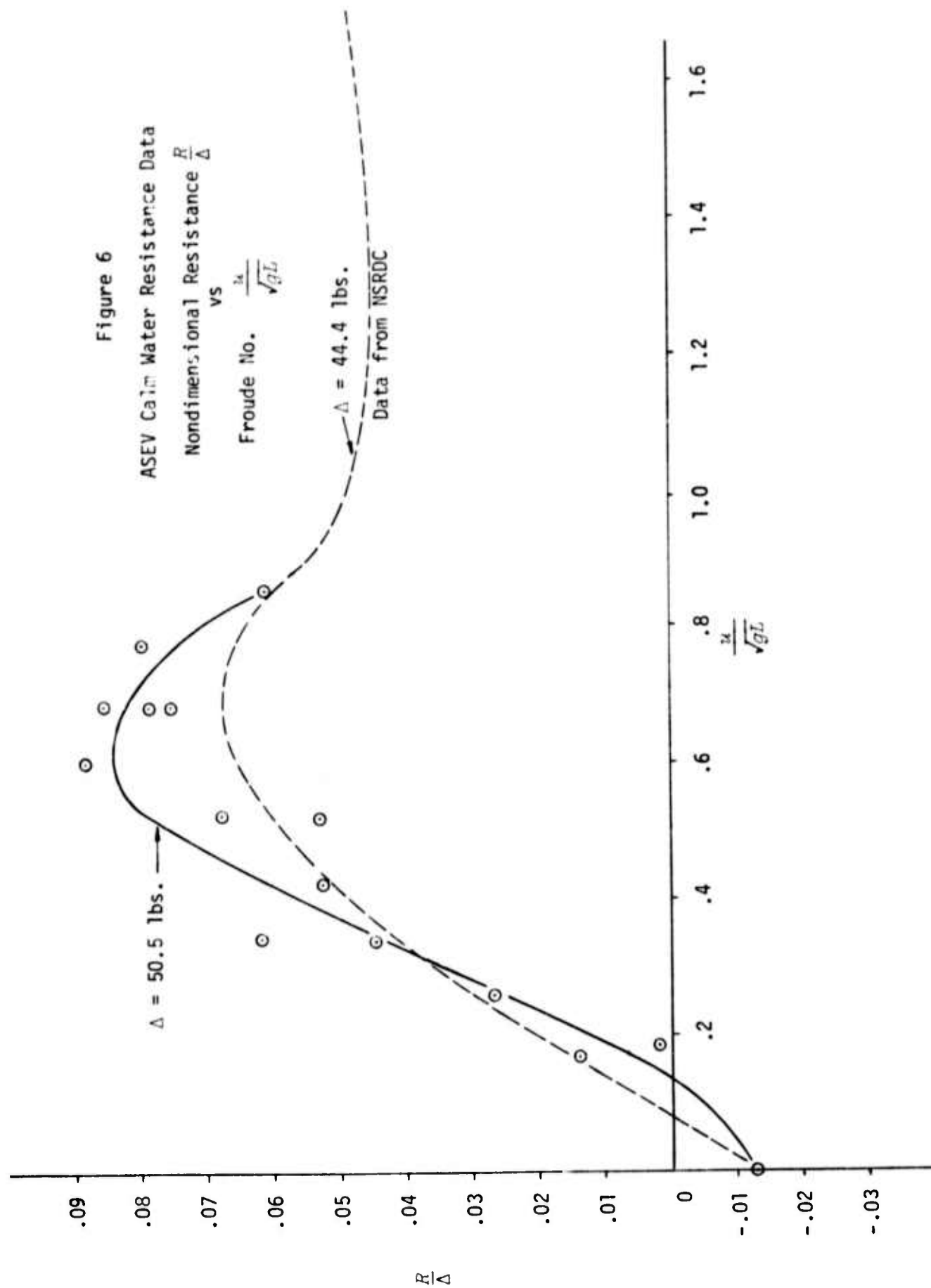
** For roll, positive indicates roll to starboard.

Figure 6

ASEV Calm Water Resistance Data

Nondimensional Resistance $\frac{R}{\Delta}$

vs

Froude No. $\frac{u}{\sqrt{gL}}$

$\Delta = 44.4$ lbs.

Data from NSRDC

$\Delta = 50.5$ lbs.

$\frac{u}{\sqrt{gL}}$

$\frac{R}{\Delta}$

ARCTEC, Incorporated

- 32 -

Skirt Friction Tests

Skirt friction tests were performed to determine if the drag of
the skirt on the model ice was causing the unstable behavior in thin ice.
Two sets of tests were conducted. The first was with the flying model,
and the second was using a sample of the model skirt material.

To conduct the tests with the flying model, a rigid platform was
constructed in the model basin using 1/2-inch plywood over a 2 by 6
frame. Series of tests were run with the platform covered with ploy-
ethylene plastic sheet and with the platform covered with the model ice
material. During each series, the model was tested at its normal trim
condition and again trimmed down-by-the-bow one degree. The results
of these tests are presented in Table 5 and plotted on the graphs of
Figures 7 and 8. These data show little difference in the drag for the
normal trim condition. For the down-by-the-bow condition, however,
there is a significant increase in the resistance.

The second set of tests was to determine the friction factor between
the model skirt material and the ice. These tests were conducted by
pulling small pieces of ice over the skirt material. Both saline ice
and the model ice were used in the tests. Weights were added to the
ice pieces in order to vary the normal force. Tests were run over
a range of velocity from 0.075 to 0.90 cm/sec. The data from these tests
are in Table 6 and are plotted in Figure 9.

Table 5
Skirt Friction Test Data

Run No.	Location of CG	V (kts.)	u (ft./sec.)	R (lbs.)	Pitch (deg.)	Roll (deg.)	$R_0(V=0)$ (lbs.)	R/Δ	$\dfrac{u}{\sqrt{gL}}$	R_0/Δ
Polyethylene Plastic Sheet on Platform 3/12/74										
1	NOM	1.15	1.94	-0.915	+0.089	+0.39	-1.15	-.0181	0.170	-.0228
2	NOM	2.30	3.89	-0.765	0.0	+0.31	-1.12	-.0151	0.340	-.0222
3	NOM	3.50	5.92	-0.434	+0.089	+0.39	-1.07	-.00859	0.518	-.0212
4	NOM	4.63	7.82	-0.256	+0.089	+0.31	-1.04	-.00507	0.684	-.0206
5	NOM	5.83	9.85	-0.450	+0.089	+0.16	-1.31	-.00891	0.861	-.0259
6	FWD	1.15	1.94	-1.16	-0.089	0.0	-1.82	-.0230	0.170	-.0360
7	FWD	2.31	3.90	-0.989	0.0	+0.15	-1.82	-.0196	0.341	-.0360
8	FWD	3.49	5.90	-0.972	0.0	0.0	-1.88	-.0193	0.516	-.0372
9	FWD	4.62	7.80	-0.710	+0.04	+0.46	-1.92	-.0141	0.682	-.0380
10	FWD	5.76	9.72	-0.550	+0.13	+0.23	-1.81	-.0109	0.850	-.0358
Model Ice Material on Platform 3/13/74										
1	NOM	1.14	1.93	-0.859	+0.089	+0.62	-	-0.0170	0.169	-
2	NOM	2.26	3.81	-0.873	+0.222	+0.77	-0.99	-0.0173	0.333	-.0196
3	NOM	3.48	5.88	-0.689	+0.222	+0.85	-1.02	-0.0136	0.514	-.0202
4	NOM	4.62	7.80	-0.504	+0.355	+0.62	-1.19	-0.0100	0.682	-.0236
5	NOM	4.05	6.84	-0.618	0.0	+0.39	-1.14	-0.0122	0.598	-.0226
6	NOM	5.17	8.73	-0.604	+0.044	+0.774	-1.18	-0.0120	0.763	-.0234
7	FWD	1.13	1.91	-0.767	-0.444	+0.310	-1.58	-0.0152	0.167	-.0313
8	FWD	2.29	3.87	-0.469	-0.488	+0.542	-1.93	-0.00929	0.338	-.0382
9	FWD	3.42	5.77	-0.085	-0.577	+0.387	-1.85	-0.00168	0.504	-.0366
10	FWD	4.62	7.80	-0.036	-0.444	+0.232	-	-0.00071	0.682	-

Δ = 50.5 lbs.

L = 4.06 ft.

ARCTEC, Incorporated

Figure 7   Skirt Friction Data, Nominal Trim Condition
            SEV Model Flown Over Rigid Platform
            Nondimensional Resistance vs. Froude No.

⊙ Polyethylene Plastic on the Rigid Platform

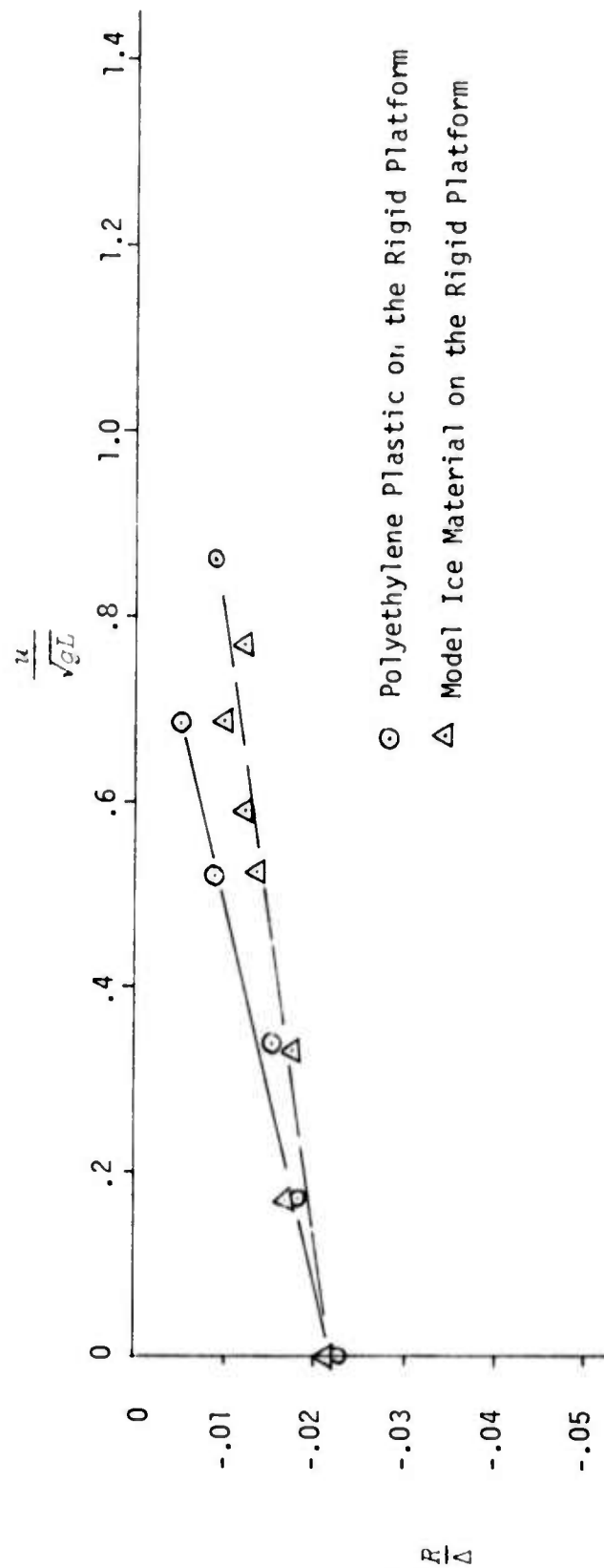△ Model Ice Material on the Rigid Platform

Figure 8   Skirt Friction Data, Center of Gravity Shifted Forward
            SEV Model Flown over Rigid Platform
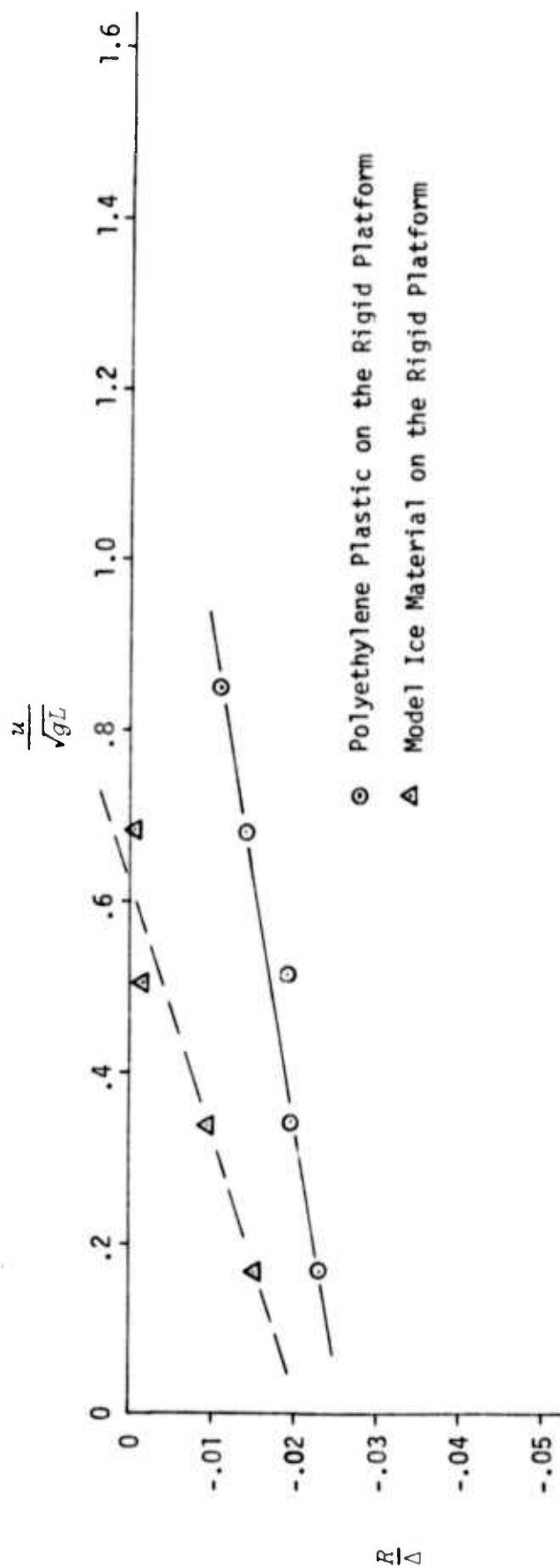   Nondimensional Resistance vs. Froude No.

Table 6

Friction Factor Tests

Test No.	N (grams)	F (grams)	V (cm./sec.)
Saline Ice Tests 5/1/74			
1	144	16.2	.075
2	144	18.7	.450
3	144	20.0	.900
4	154	15.1	.075
5	154	27.7	.450
6	154	27.3	.900
7	508	50.9	.075
8	508	62.9	.450
9	508	77.4	.900
10	110	10.1	.075
11	110	13.3	.450
12	110	14.9	.900
13	316	30.1	.075
14	316	41.8	.450
15	316	48.6	.900
Model Ice Tests 5/2/74			
1	297	59.8	.075
2	297	68.8	.450
3	297	59.0	.900
4	97	40.7	.075
5	97	28.6	.450
6	97	33.6	.900
7	497	85.9	.075
8	497	101.	.450
9	497	96.9	.900
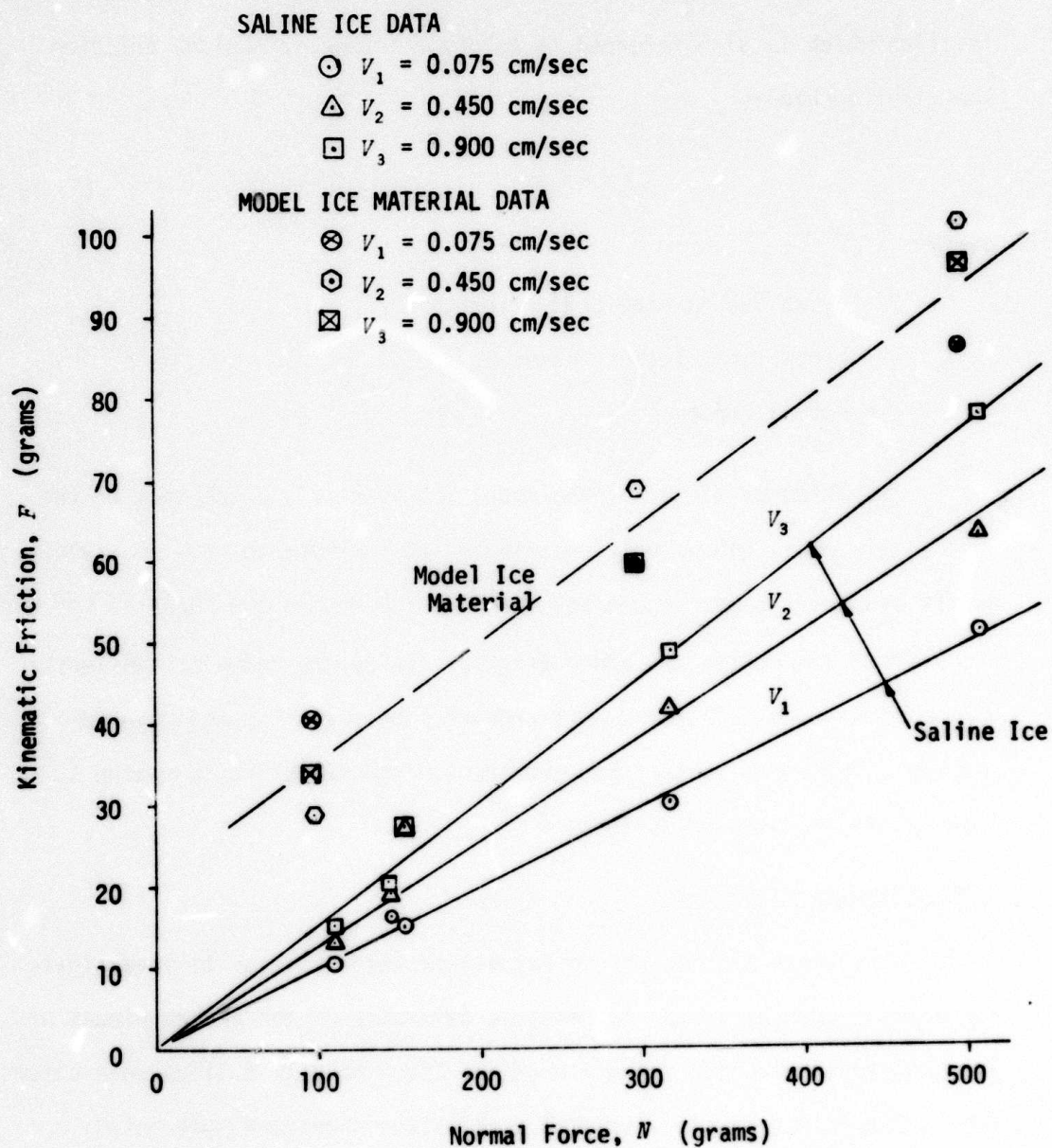
Figure 9   Friction Factor Test Results.

ARCTEC, Incorporated

- 38 -

The data was analyzed using the familiar model for kinematic
friction which is also referred to as dry friction or coulomb friction.
The relationship is

$$F = \mu N \tag{9}$$

where

F = force due to kinematic friction

μ = kinematic friction factor

N = normal force

The friction factor of the model ice is nearly twice that of the
saline ice. This undoubtedly contributed to the nose-in problem experienced
As the bow skirt comes in contact with the ice due to the shape of the wave
in front of the craft, the added friction causes the nose-in. While the
added friction contributes to the problem, the fact that the wave in
the ice resulted in contact between the ice and bow skirt is reason to
investigate the problem further.

Icebreaking with the SEV

While the purpose of the resistance tests was not to investigate
icebreaking per se, it was intended to determine if the broken pieces of
ice interfered with the operation of the SEV. No difficulties were observed
during the tests; however, several interesting phenomena were noted.

Icebreaking occurred in two ways. At low speed the ice was observed

to fail because the cushion pressure depresses the water under the ice sheet in the vicinity of the vehicle and large sections are left unsupported. The ice then breaks of its own weight. This only occurred in thin ice and will depend on the cushion pressure as well as the thickness of the ice. The photographs in Figures 10 and 11 show model ice broken during low speed tests.

At speeds in the vicinity of the critical velocity, the ice would crack because of the wave generated by the moving craft. The amount of damage to the ice appeared to be less than in the slow speed case. Both the low speed and high speed icebreaking phenomena have been observed in recent tests of full scale SEV's as was reported in Reference 6. (A copy of Reference 6 is included as Appendix A.)

Figure 10.   Broken Ice After Slow Speed Operation

Figure 11.   Channel Broken by ASEV at Slow Speed

Conclusions and Recommendations

The objective of the resistance tests was achieved in that it was demonstrated through model testing that the resistance of an SEV operating over ice is a function of the mechanical properties of the ice sheet. In particular, there is a peak resistance which occurs in the vicinity of the critical velocity of the flexural waves in the ice sheet. The peaks, however, were found to be less than the primary hump in calm water and decrease with increasing ice thickness.

An unstable condition was observed when operating in thin ice near the critical velocity. The shape of the wave generated in the ice sheet under the craft was such that it came in contact with the bow skirt. Friction between the skirt and the model ice caused the model SEV to pitch down by the bow. Notwithstanding the fact that the testing was performed with the model restrained in surge and that the skirt friction over the model ice is high, this phenomenon requires further investigation.

It is, therefore, recommended that additional testing be performed specifically to investigate the interaction between the skirt system of the SEV with the wave generated in the ice sheet. This investigation should include several models in order to determine the effects of variation of the beam to length ratio.

ARCTEC, Incorporated

- 43 -

IV. PARKING TESTS

Objective

As part of the total model testing program, four days of testing
were devoted to performing parking tests. The purpose of this testing
was to form a basis upon which to design a landing pad configuration
to enable an Arctic SEV to park on the ice. In forming this basis two
areas were of particular interest. The first was to observe the manner
in which the ice failed for a given landing pad configuration, and the
second was to determine empirically the bearing capacity of the ice as
a function of the ice thickness and ice properties for different landing
pad configurations. The best landing pad configuration corresponds to
the one which permits the Arctic SEV to park on the thinnest ice
without the ice failing in some manner.

From discussions with the Arctic SEV Program Office, the
following five (5) configurations, which are depicted in Figures 12
through 16 for a 170-ton craft, were chosen to be tested:

- Four Hard Pads
- Runners
- Inflated Rectangular Pad
- Four Inflated Pads
- Inflated Circular Pad

These configurations, with the exception of the circular pad, were selected
based on preliminary design considerations and on design work going on

Figure 12. Four Hard Pads

Buttock in Inches
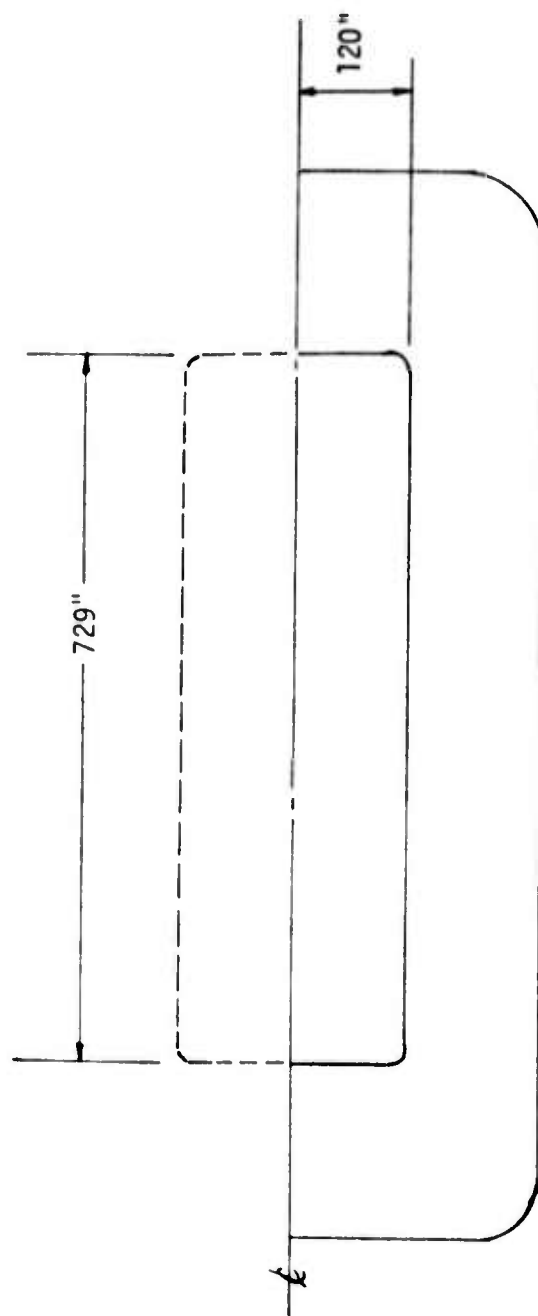
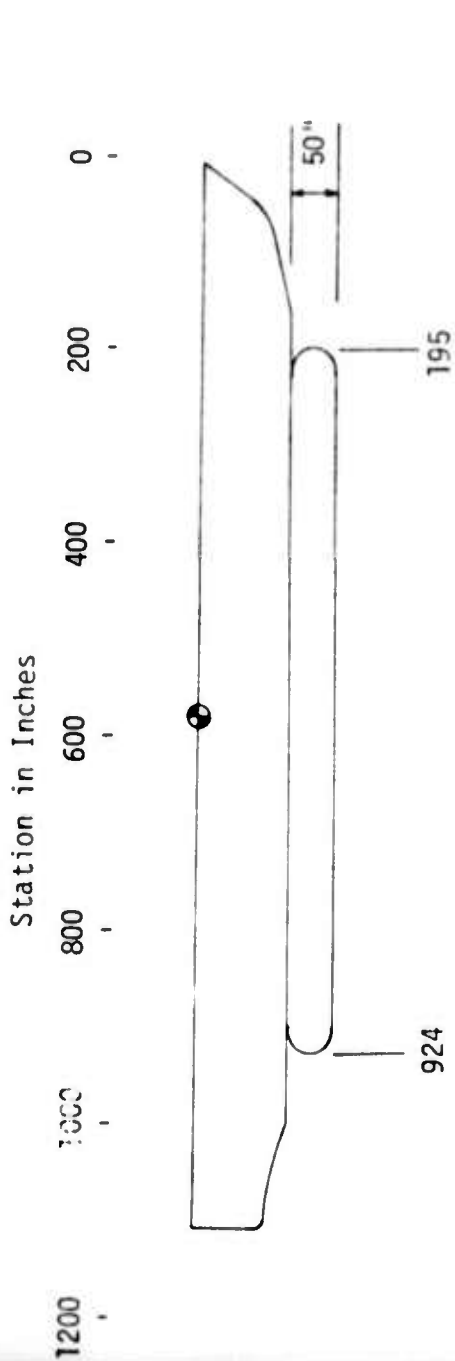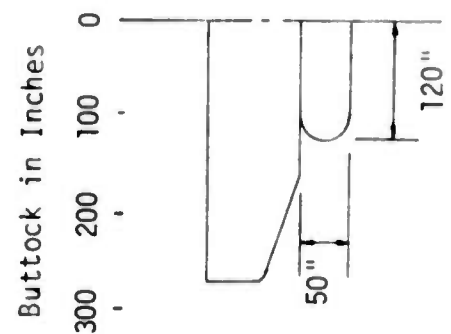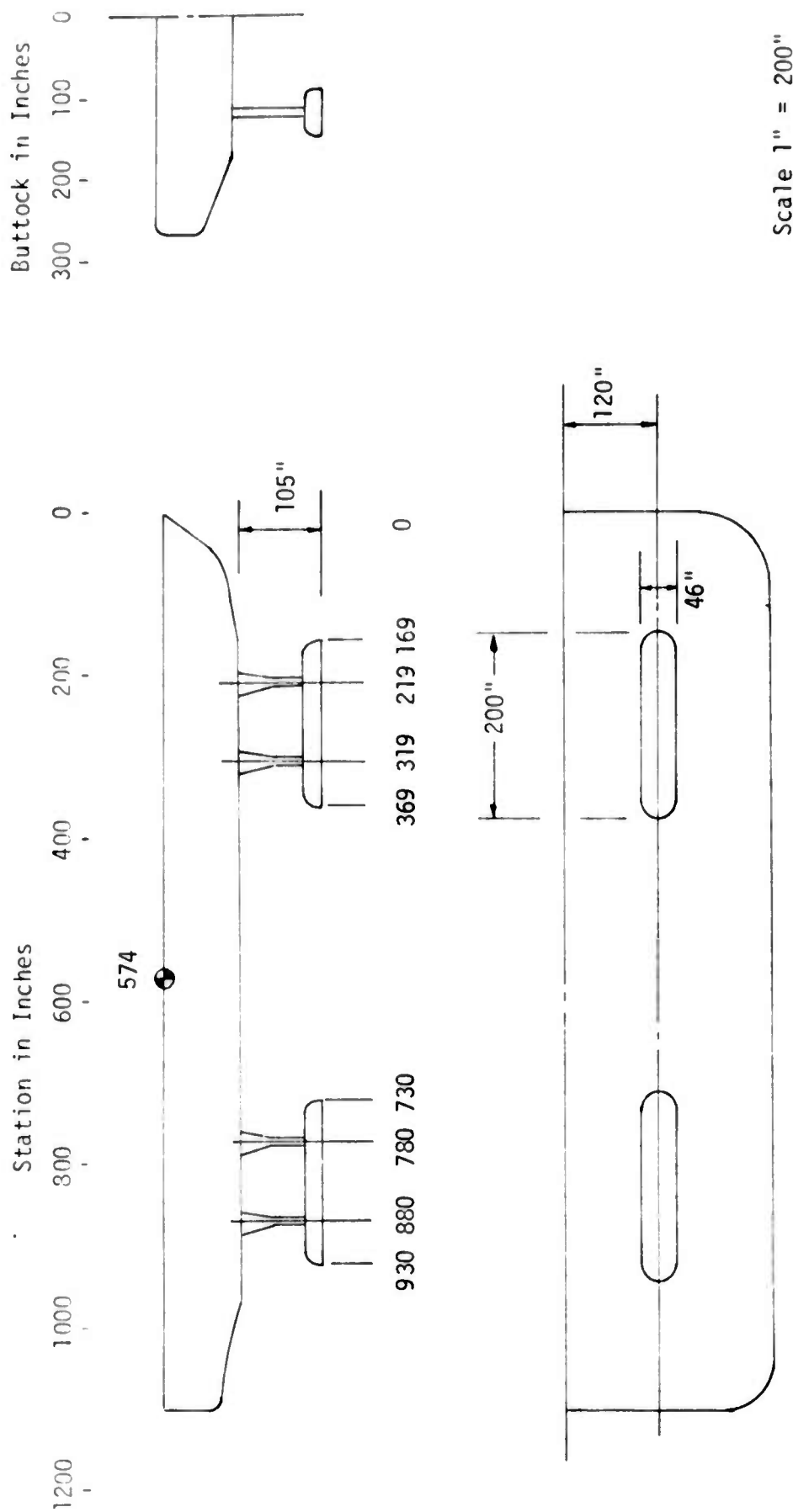Station in Inches

Scale 1" = 200"
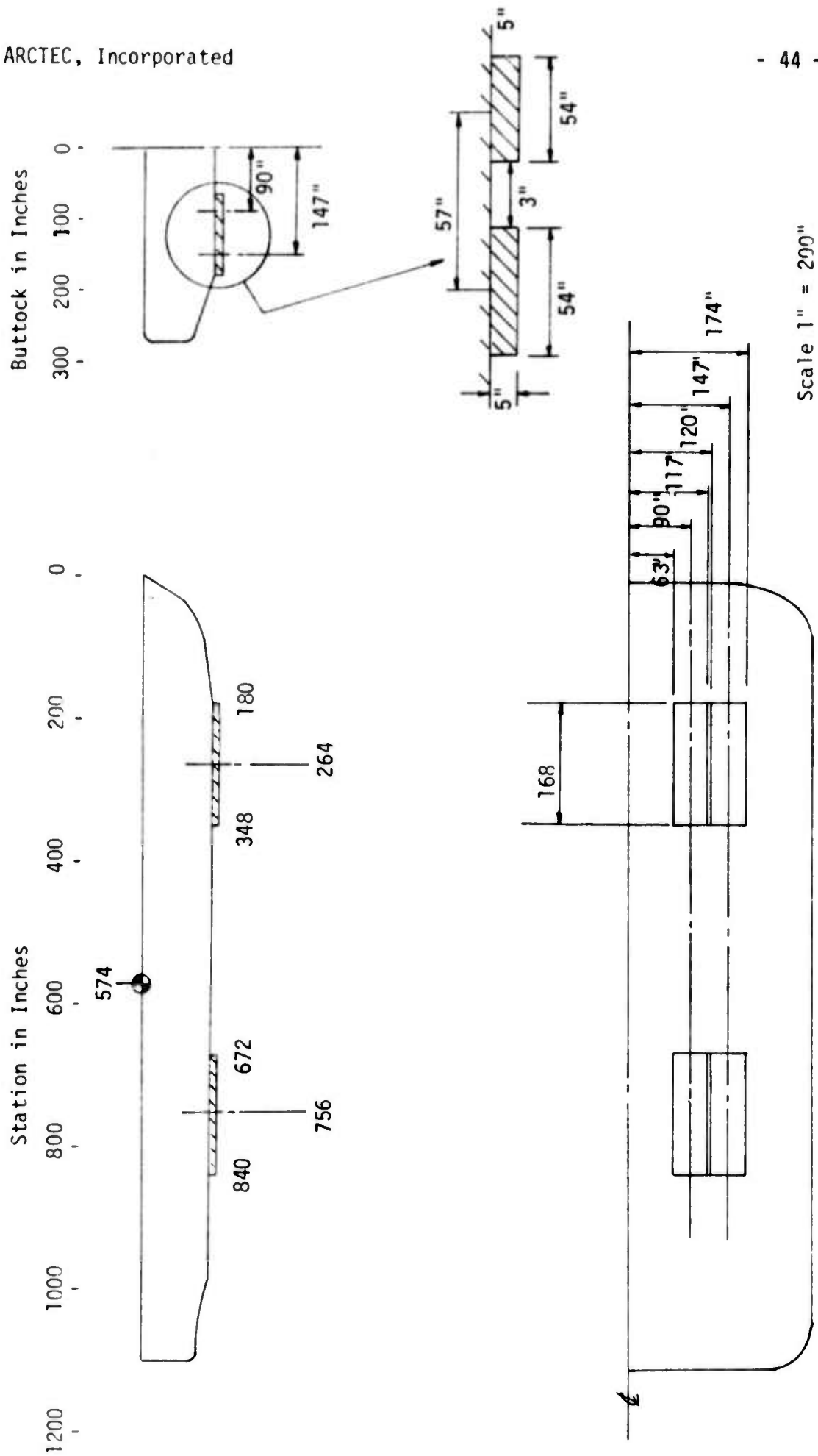
Figure 13. Runners
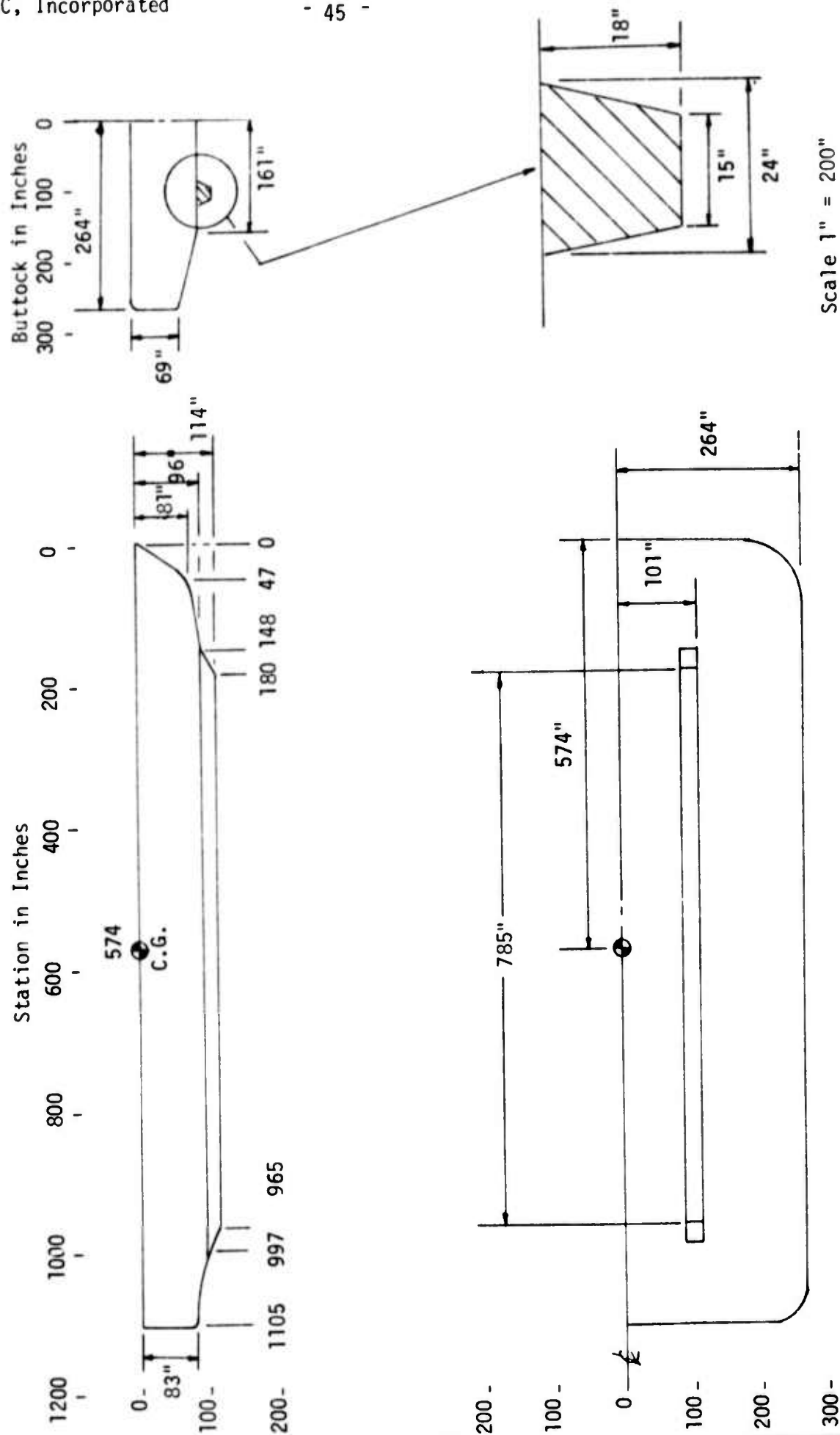
Scale 1" = 200"

Figure 14. Inflated Rectangular Pad

Figure 15. Four Inflated Pads

Scale 1" = 200"

- 48 -

Figure 16. Circular Inflated Pad

50"

473"

Scale 1" = 200"

ARCTEC, Incorporated

- 49 -
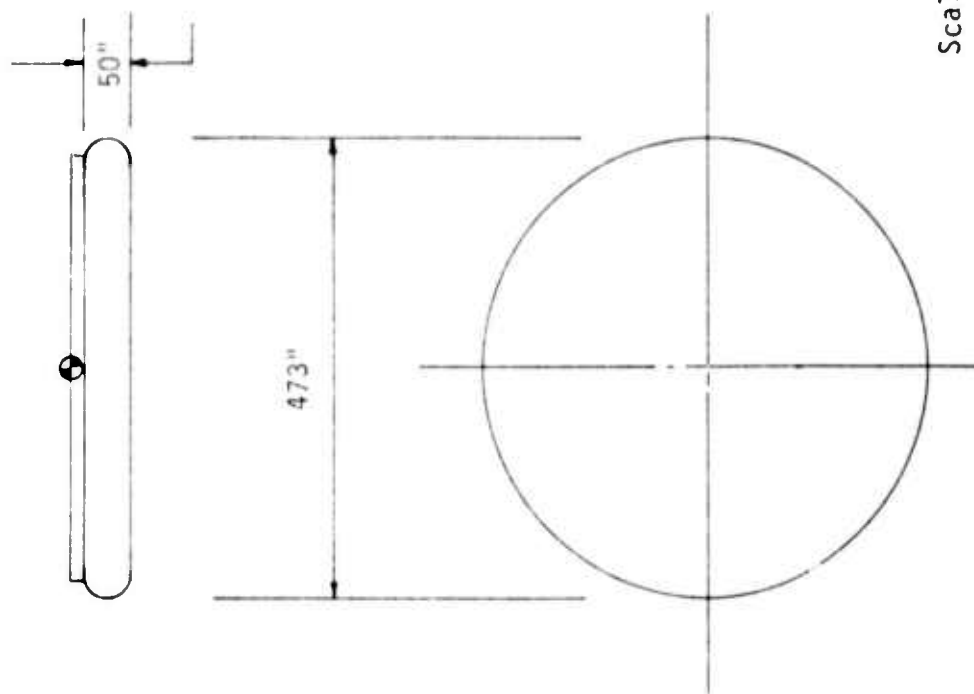
elsewhere. The actual dimensions of each of these configurations are
based primarily upon the particular design of the craft with constraints
imposed due to the basic structural design and imposed to prohibit the
supports from interfering with the operation of the craft. As an aid
in developing empirical expressions for the bearing capacity, the
circular pad was proposed as an additional test configuration because
of its radial symmetry. The load area for the circular pad was chosen
to be the same as that of the rectangular pad. Using these designs for
the 170 ton craft, models of each were constructed of plexiglas with
foam rubber used to represent the inflated pads. A scale factor of
19 was selected in constructing and testing these models to enable the
results of these parking tests to correspond directly to the model
used for the flying tests.

Test Procedure

The test program consisted of determining the bearing capacity of
the ice as a function of the craft size, size and shape of the landing pads
and the thickness and properties of the ice. Using these results, the
minimum required ice thickness to support a full-scale craft can be established
for the different landing pad configurations. The minimum of these corres-
ponds to the best configuration, that is, the one which permits the craft
to park on the thinnest ice without the ice failing.

The overall test plan consisted of testing all five models in four
MOD-ICE sheets of various thicknesses and properties. In addition, two
of these data points were duplicated by testing the model with the four
inflated pads twice in two of the sheets yielding a total of twenty-two
(22) data points.

For each test, the following variables were either measured, calculated, or recorded:

- h ~ sheet thickness

- σ_f ~ flexural strength of sheet

- E ~ elastic modulus of sheet

- ℓ ~ characteristic length = $\left(\dfrac{Eh^3}{12\rho_w g(1-\nu^2)}\right)^{1/4}$

- P ~ load trace

- Failure Crack Pattern

- Dimensions of Failure Pattern

A typical testing sequence began with the elastic modulus measurement. This measurement was pe   d by depressing the sheet at a constant deflection rate while recording the magnitude of the corresponding load and deflection of the sheet a specified distance away from the load. From this record, along with the sheet thicknesses, the elastic modulus was calculated using the standard force-deflection relation for a plate on an elastic foundation. Following the elastic modulus measurement, the first model was attached to a specially machined, hollow steel force block which is suitably instrumented with semi-conductor strain gages to sense the applied loads. The model was then positioned at a selected location as depicted in Figure 17. The model was then slowly lowered at a constant deflection rate to represent an SEV gradually parking. As the model began to depress the sheet, the output signal from the force block, which is proportional to the load applied to the
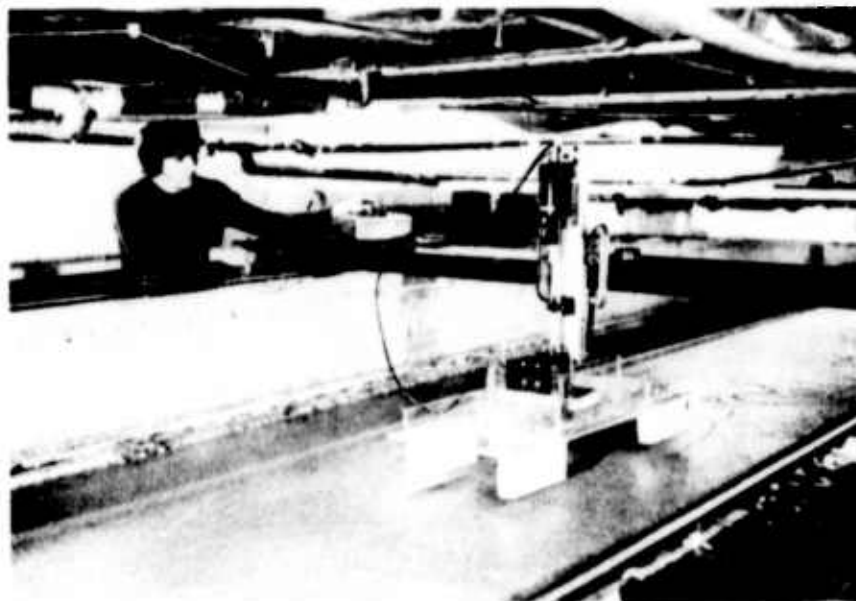
ARCTEC, Incorporated

- 51 -

Figure 17. Parking Test Set-Up

ARCTEC, Incorporated

- 52 -

model by the sheet, was amplified and recorded permanently on an oscillo-
graph recorder. The constant deflection rate was continued until a
complete breakthrough failure occurred at which time the force began
to decrease. The model was then disconnected from the force block and
the next model connected. While this was being done, the failure pattern
including appropriate dimensions and sheet thicknesses were recorded.
Also, black and white prints were taken of the failure pattern in order
to have a permanent record of the pattern. The same procedure was then
repeated for the next model. After all the models had been tested, the
force block was calibrated to insure proper correlation with the applied
model forces. Following the testing of the models, the flexural strength
of the MOD-ICE sheet was measured by breaking insitu cantilever beams.

Test Results and Analysis

A summary of the test data is presented in Table 7. From the
oscillograph record of the load trace, two loads were extracted. The
first was the load which caused the first crack to appear (P_1) and the
second was the maximum load (P_{max}) which corresponds to a complete break-
through failure of the sheet. The typical crack pattern and load trace
for each model are sketched in Figures 18 through 22. In addition, the
dimensions of the crack pattern for each test are tabulated in each of
these figures.

The mode of failure for each model test followed the same general
sequence. The models were slowly lowered at a constant deflection rate.
As the models came in contact with and began to depress the sheet, the

Table 7
Results of Parking Tests

DATE	MODEL	h (cm)	σ_f (kg/cm²)	E (kg/cm²)	ℓ (cm)	P_1 (kg)	P_{max} (kc)	$\frac{L_b^{**}}{\ell}$	$\frac{P_1}{\sigma_f \ell^2}$	$\frac{P_{max}}{\sigma_f \ell^2}$
4-9-74	4*	1.50	.256	446.	19.4	6.48*	8.80*	5.86	11.24*	15.29*
	2	1.53			19.7	7.54	10.19	5.77	12.58	17.00
	3	1.55			19.9	7.54	14.16	5.72	12.26	23.02
	1	1.52			19.6	12.69	17.69	5.80	21.46	29.91
	4*	1.54			19.8	7.33*	9.06*	5.74	12.08*	14.93*
	5	1.46			19.0	6.74	11.58	5.98	12.35	21.22
4-16-74	4	2.11	.235	544.	26.3	----	14.43	4.32	----	14.15
	3	2.10			26.2	9.25	22.94	4.33	9.16	22.72
	5	2.21			27.2	11.10	17.95	4.17	9.92	16.05
	2	2.28			27.9	12.12	19.15	4.07	10.18	16.09
	1	2.26			27.7	22.02	33.30	4.10	18.83	28.47

(continued)

Table 7 continued

Results of Parking Tests

DATE	MODEL	h (cm)	σ_f (kg/cm²)	E (kg/cm²)	ℓ (cm)	P_1 (kg)	P_{max} (kg)	$\frac{L_D**}{\ell}$	$\frac{P_1}{\sigma_f \ell^2}$	$\frac{P_{max}}{\sigma_f \ell^2}$
4-18-74	2	2.63	.179	640.	32.3	13.36	20.24	3.51	10.79	16.35
	1	2.73			33.2	23.60	31.84	3.42	17.69	23.87
	3	2.78			33.7	12.80	24.72	3.37	9.25	17.87
	4	2.96			35.3	-----	17.60	3.22	-----	11.22
	5	3.05			36.1	14.00	21.36	3.14	8.41	12.83
4-22-74	3	2.31	.162	444.	26.8	5.23	10.80	4.24	6.05	12.49
	4*	2.19			25.7	-----	6.53*	4.42	-----	8.40*
	5	2.10			24.9	8.00	14.34	4.56	11.20	20.07
	4	2.09			24.8	6.59	10.30	4.57	9.31	14.56
	1	2.07			24.6	16.37	24.28	4.61	23.58	34.98
	2	2.11			25.0	9.39	12.91	4.54	13.02	17.90

NOTE: Model No. 1 ~ Four Hard Feet
        "   2 ~ Runners
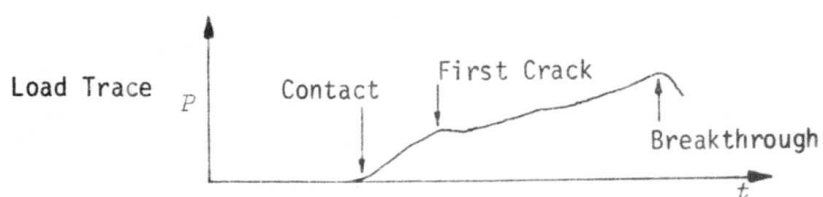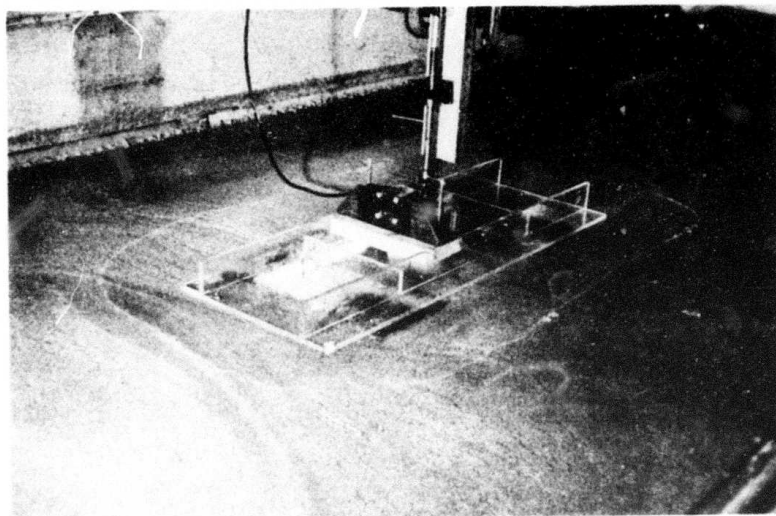   "   3 ~ Inflated Rectangular Pad
        "   4 ~ Four Inflated Pads
        "   5 ~ Inflated Circular Pads

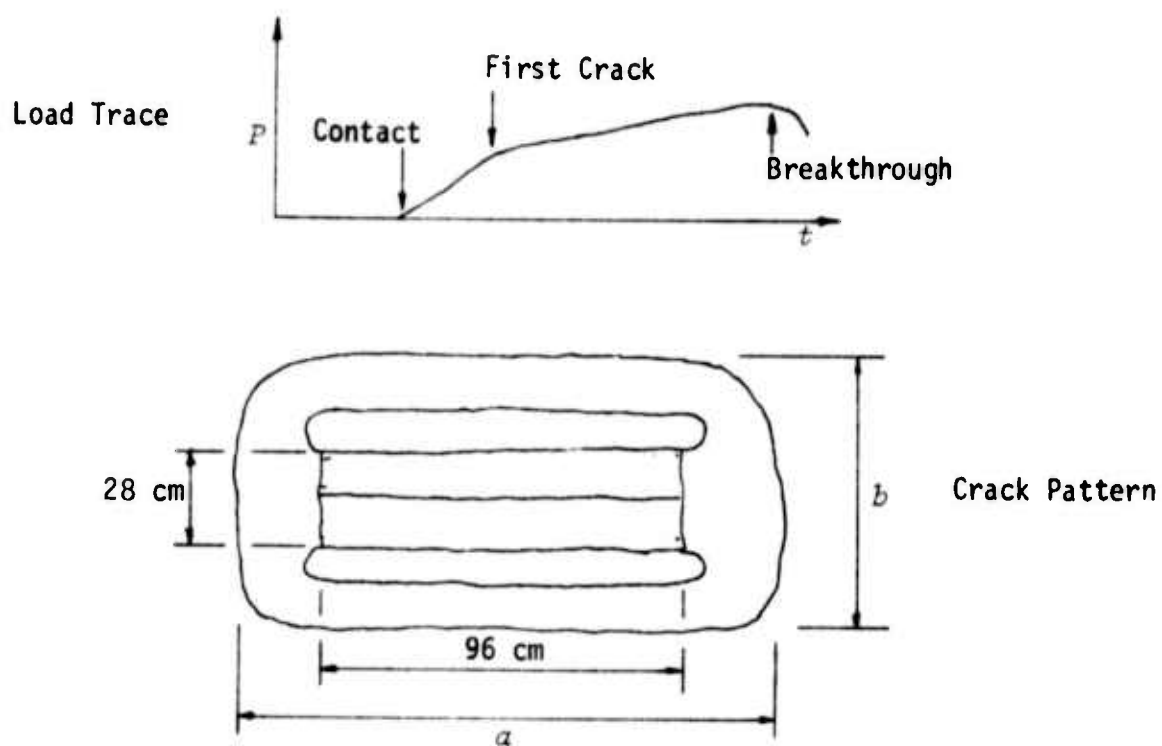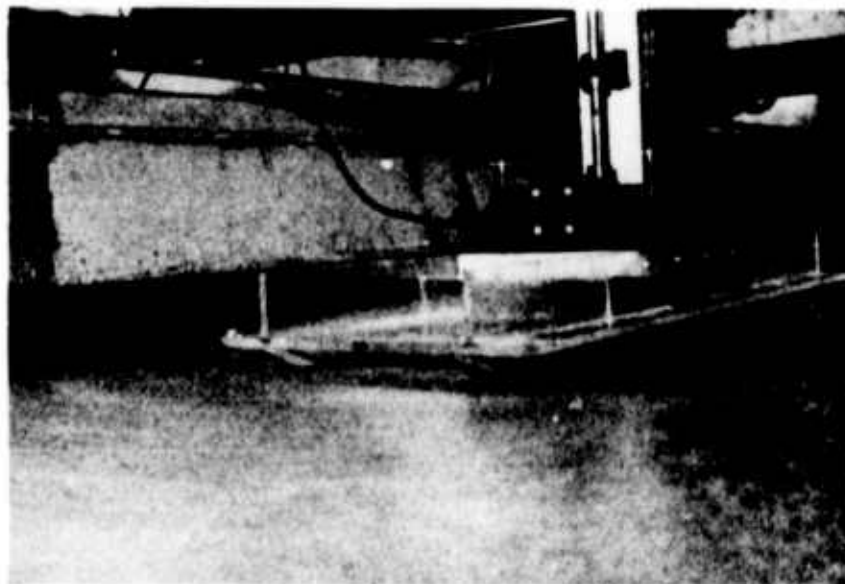* Aft C.G.: Forces reported are adjusted upwards (8.8%) to correspond to center C.G. condition.

**L_D = 113.5 cm for models tested.
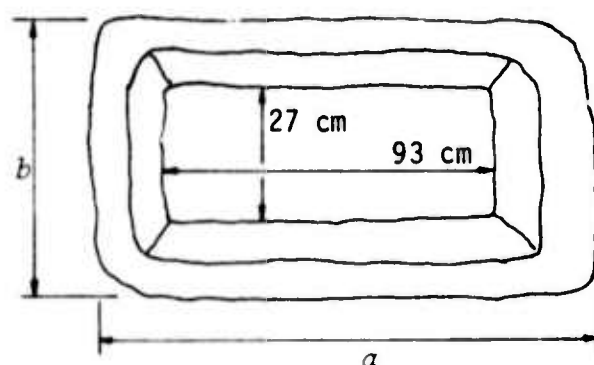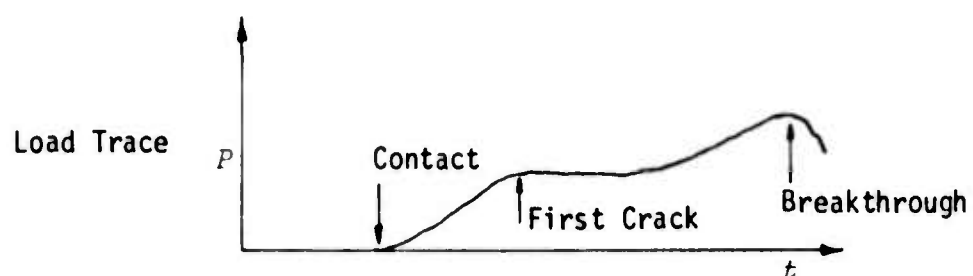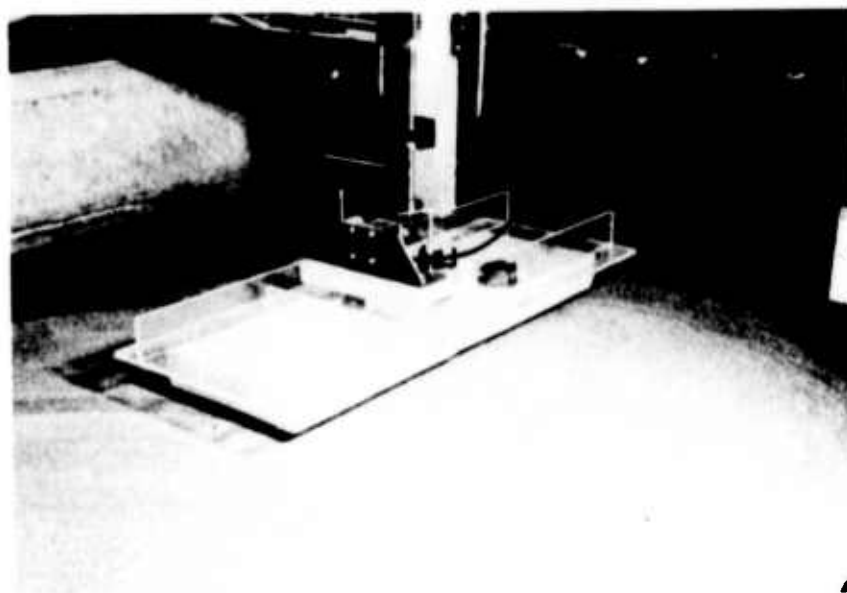
Figure 18

Failure Pattern for Four Hard Pads Model

Load Trace

Crack Pattern
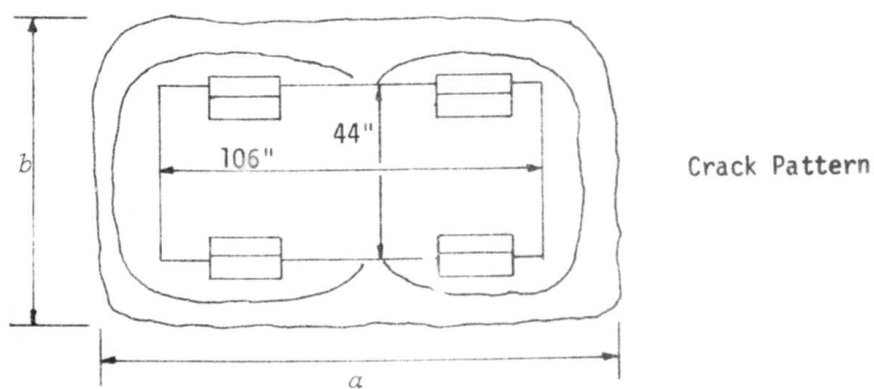
Test Day	a(cm)	b(cm)
4-9-74	143.5	80.
4-16-74	155.	93.
4-18-74	160.	100.
4-22-74	144.	91.

Figure 19
Failure Pattern for Runners Model

Load Trace

Crack Pattern

Test Day	a(cm)	b(cm)
4-9-74	132.	70.5
4-16-74	138.	85.
4-18-74	145.	90.
4-22-74	139.	79.

Figure 20
Failure Pattern for Inflated Rectangular Pad Model

Load Trace

Crack Pattern

Test Day	a(cm)	b(cm)
4-9-74	127.	90.
4-16-74	129.	86.
4-18-74	142.	87.
4-22-74	127.	74.

Figure 21

Failure Pattern for the Four Inflated Pads Model
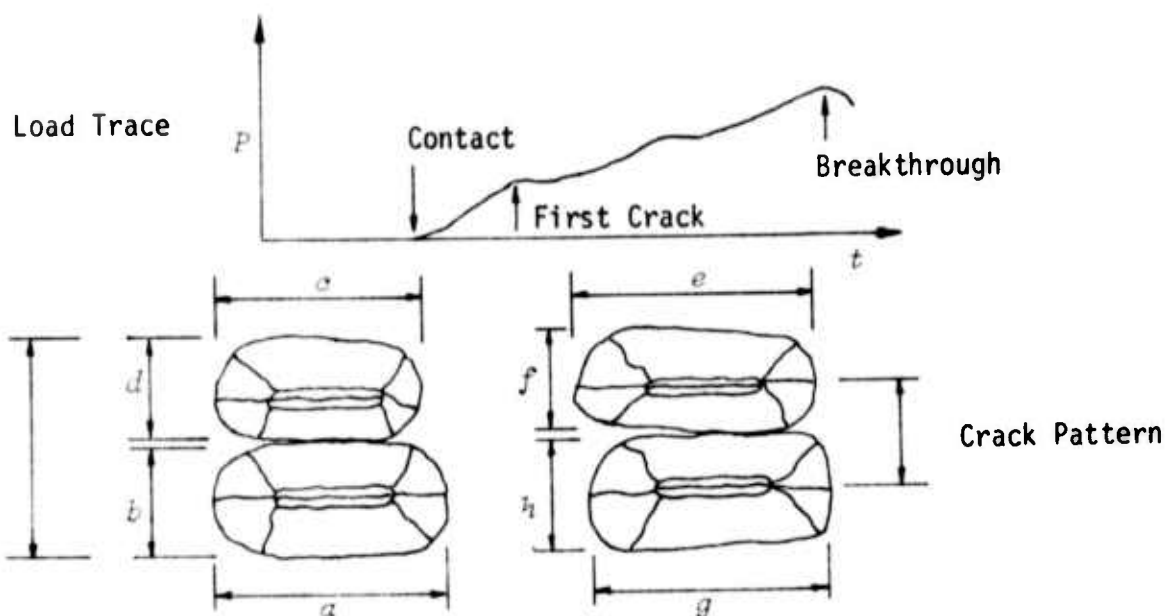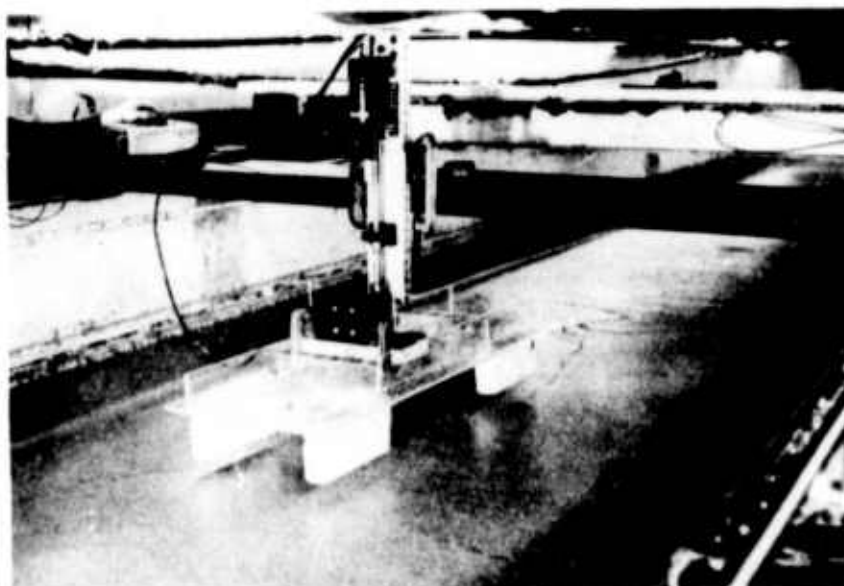
Test Day	a(cm)	b(cm)	c(cm)	d(cm)	e(cm)	f(cm)	g(cm)	h(cm)
4-9-74*	-	-	-	-	-	-	-	-
4-9-74*	-	-	-	-	10.5	28.	39.	25.5
4-16-74	53.	38.	53.	37.5	45.	27.	42.	33.
4-18-74**				n.a.				
4-22-74*	-	-	-	-	44.	30.	41.	29.
4-22-74	56.	-	56.	-	50.	35.	55.	35.

*   ~ aft c.g. location
** ~ Failure Pattern occurred as large circumferential cracks about the
        two bow pads and two aft pads. Dimensions for these cracks were
        61 cm x 81 cm and 63 cm x 77 cm.

Figure 22
Failure Pattern for the Inflated Circular Pad Model
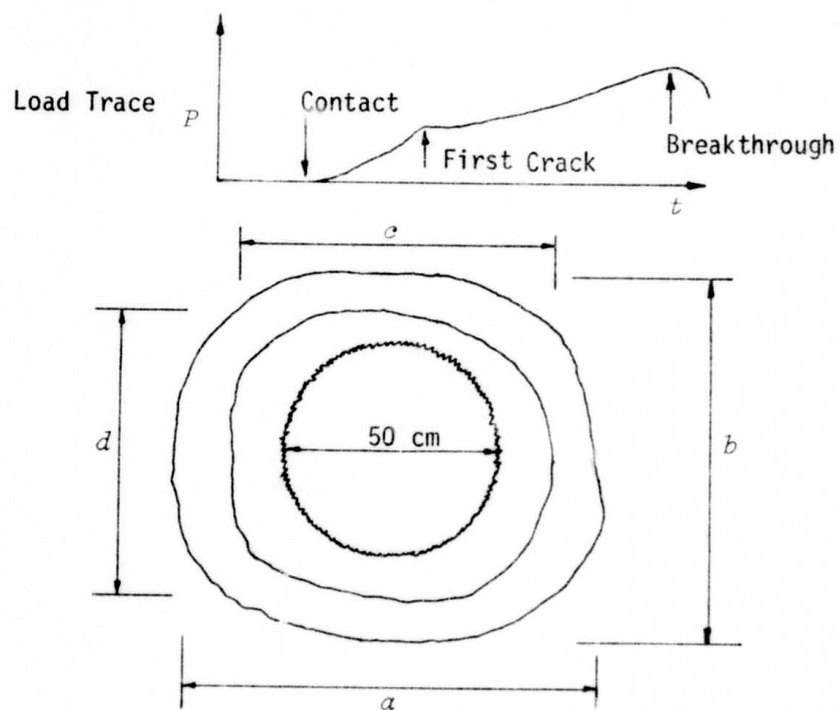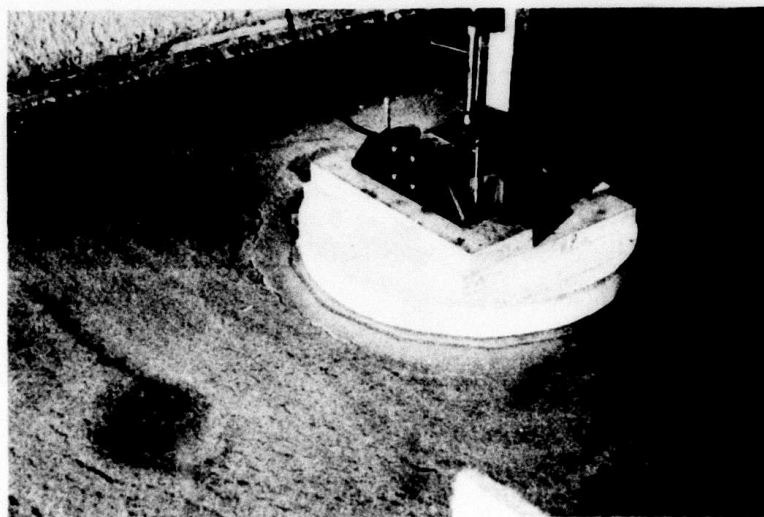
Test Day	a(cm)	b(cm)	c(cm)	d(cm)
4-9-74	94.	96.5	61.	61.
4-16-74	-	-	77.	79.
4-18-74	106.	115.	95.	83.
4-22-74	88.	97.	76.	72.

force increased in a linear manner with increasing deflection. This
continued until the load increased to P_1 and a large circumferential
crack (first crack) appeared. As the motion continued beyond this point,
the force continued to increase but at a lower rate. With further
deflection, additional cracks began to appear until a complete break-
through failure occurred and the load began to decrease. This failure
usually corresponded to a second circumferential crack located between
the boundary of the model and the first outer circumferential crack.

In analyzing the failure sequence, the bearing capacity can be
defined as either the load to cause the first crack to appear (P_1) or
as the load to cause complete breakthrough failure (P_{max}). The analysis
presented in this section treats both. The bearing capacity, whether
it is characterized by P_1 or by P_{max}, can be expressed in the following
functional form for each model:

$$P_1 = f_1(h, \sigma_f, E)$$
$$P_{max} = f_2(h, \sigma_f, E)$$

(10)

where

P_1 = load required to cause the first crack to appear

P_{max} = load required to cause complete breakthrough failure

h = ice thickness

σ_f = ice flexural strength

E = elastic modulus of ice

In order to replace the above functional equations with empirical ones,
either of two approaches can be used to analyze the test results. The

first is to analyze the data in its dimensional form. Using this method
each independent variable (h, E and σ_f) must be investigated in turn to
determine the corresponding influence on the dependent variables (P_1 and
P_{max}). Because of the limited amount of data, this approach proves to
be extremely difficult if not impossible. The second approach is to
use dimensional analysis. To use this method, equations (10) must be
transformed into appropriate non-dimensional ones. To accomplish this,
consider the mode of failure which can be described as bending
failures occurring when bending stress at the outer fibers of the sheet
equal the flexural strength σ_f. From elementary plate theory, the maximum
bending stress can be expressed as:

$$\sigma_{max} = \frac{M_{max}}{6h^2} \tag{11}$$

where M_{max} = maximum bending moment per unit length. For a plate
on an elastic foundation, M_{max} can be expressed as:

$$M_{max} = P \times f_3 \left(\frac{\xi}{\ell}\right) \tag{12}$$

where ξ is some designated parameter which describes the size of the load
area. As an example, the parameter ξ for a small uniform circular load is
defined as the radius of the load area. Substituting equation (12) into
equation (11) yields

$$\sigma_{max} = \frac{P}{6h^2} \times f_3 \left(\frac{\xi}{\ell}\right) \tag{13}$$

ARCTEC, Incorporated

or rearranging

$$\frac{P}{\sigma_{max}h^2} = \frac{6}{f_3(\frac{\xi}{\ell})} = f_4(\frac{\xi}{\ell}) \tag{14}$$

Using this equation as a basis, equations (10) can be transformed into the following non-dimensional ones:

$$\frac{P_1}{\sigma_f h^2} = f_5(\frac{\xi}{\ell}) \tag{15}$$

$$\frac{P_{max}}{\sigma_f h^2} = f_6(\frac{\xi}{\ell}) \tag{16}$$

where $\frac{P_1}{\sigma_f h^2}$, $\frac{P_{max}}{\sigma_f h^2}$ = non-dimensional bearing capacities

(ξ/ℓ) = non-dimensional load size

To proceed from this point, the parameter ξ must be defined. Because of the diversity of the models, it was decided to use the length of the flat bottom of the hull (L_b) as ξ for all the models. In this manner, ξ/ℓ corresponds to the same ice conditions and craft size for all the models. From the standpoint of comparing models, this enable the best landing pad design to correspond to the design with the highest $P/\sigma_f h^2$ at a given ξ/ℓ. Also by defining ξ as L_b, the results can easily be related to craft size, that is, a 170 ton craft, 540 ton craft, and so on. Substituting L_b for ξ, equations (15) and (16) become:

ARCTEC, Incorporated

$$\frac{P_1}{\sigma_f h^2} = f_5\left(\frac{L_b}{\ell}\right) \tag{17}$$

$$\frac{P_{max}}{\sigma_f h^2} = f_6\left(\frac{L_b}{\ell}\right) \tag{18}$$

where the functions f_5 and f_6 must be determined from the data. To determine these functions, $\frac{P_1}{\sigma_f h^2}$ and $\frac{P_{max}}{\sigma_f h^2}$ were plotted versus L_b/ℓ on log - log paper as shown in Figure 23 . From these plots, it is seen that the bearing capacity for each model can be expressed quite well by the following equations:

$$\left. \begin{array}{l} \dfrac{P_1}{\sigma_f h^2} = C_1\left(\dfrac{L_b}{\ell}\right)^{1/2} \\[3em] \dfrac{P_{max}}{\sigma_f h^2} = C_2\left(\dfrac{L_b}{\ell}\right)^{1/2} \end{array} \right\} \quad 3. \leq \frac{L_b}{\ell} \leq 6. \tag{19}$$

where C_1 and C_2 are defined by the following table for the different landing pad configurations:

| Landing Pad Configuration	C_1	C_2
Four Hard Pads	9.69	13.92
Runners	5.54	8.04
Rectangular Inflated Pad	4.86	10.09
Four Inflated Pads	4.68	6.48
Circular Inflated Pad	4.98	8.29

Parking Test Results
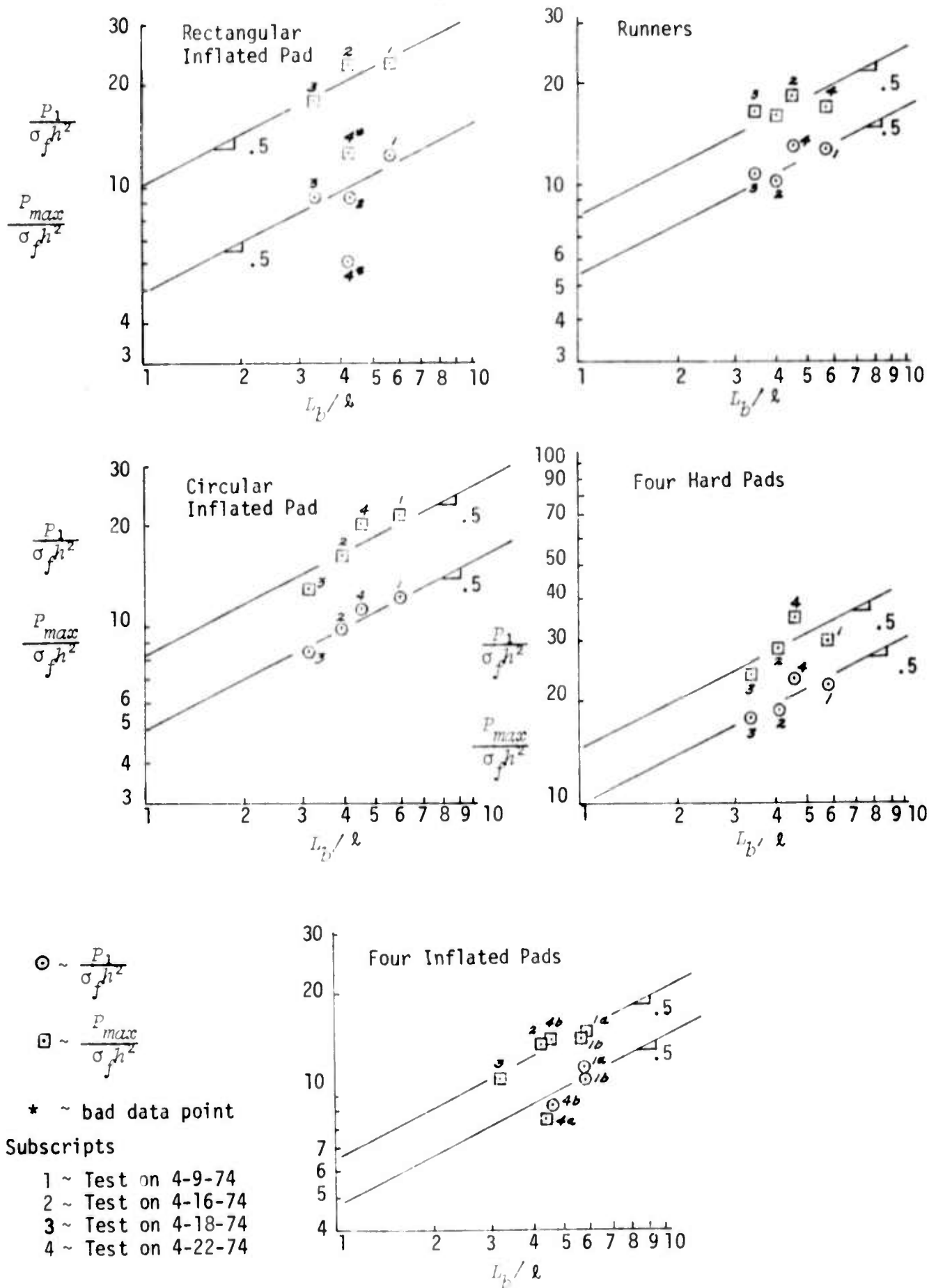
ARCTEC, Incorporated

These results are presented in graphical form in Figure 24. A discussion of these results is presented in the next section.

Figure 24
Non-Dimensional Bearing Capacities
Versus
L_b/ℓ

Landing Pad Configuration

$P_1/\sigma_f h^2$ First Crack

$P_{max}/\sigma_f h^2$ Max. Load

$(L_b/\ell)^{1/2}$

Range of Data

1.5   2.0   2.5   3.0

0   10   20   30   40   50

1   Four Hard Pads
2   Runners
3   Rectangular Inflated Pad
4   Four Inflated Pads
5   Circular Inflated Pad

$\dfrac{P_1}{\sigma_f h^2}$ $\dfrac{P_{max}}{\sigma_f h^2}$

ARCTEC, Incorporated

- 67 -
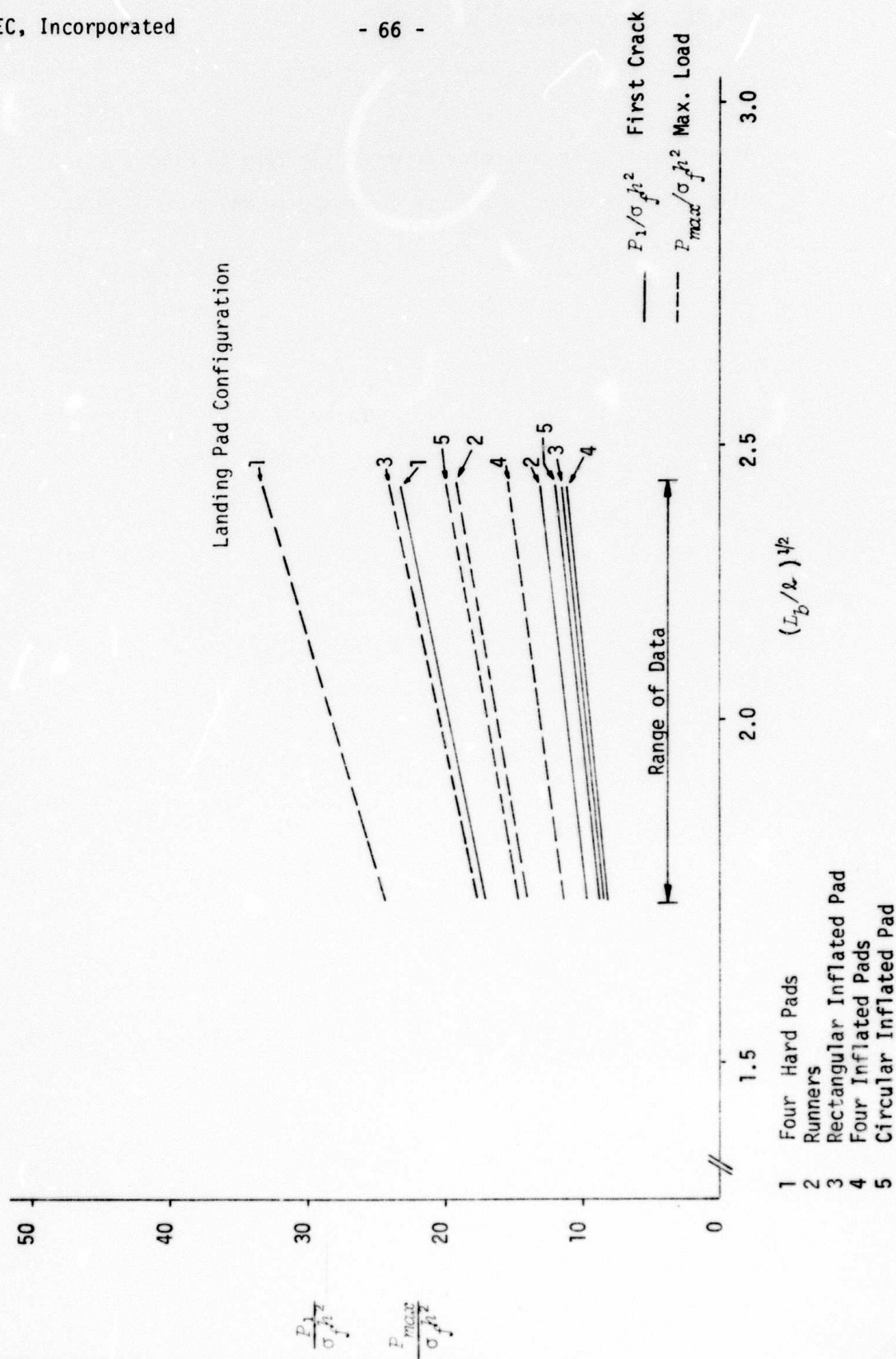
Full-Scale Prediction

The full scale predictions for the 170 ton, 540 ton and 1000 ton crafts are presented in dimensional form in Figures 25, 26 and 27 respectively. In each figure, the following two plots are shown: (1) ice thickness versus load to cause the first crack; and (2) ice thickness versus load to cause breakthrough failure of the ice. To use these plots, one enters with a known craft weight and determines the minimum ice thickness for which the failure condition will *not* occur for a particular landing pad configuration. If the ice is thinner than this value of thickness, the failure condition *will* occur while if the ice is thicker, the failure condition *will not* occur. To illustrate this further consider the 170 ton craft with an inflated rectangular pad (model number 3). From Figure 25, it is seen that if the ice is thicker than approximately 2.1 feet no cracks will occur. If the ice thickness is less than 2.1 but greater than 1.3 feet, the craft will cause cracks to appear. Finally if the ice is less than 1.3 feet thick, the craft will breakthrough the ice. Using these plots in this manner, Figures 28, 29, and 30 are presented for the three craft sizes and for each landing pad design to depict under what conditions the following three failure responses will occur:

- No Failure

- Appearance of Cracks

- Breakthrough Failure

Figure 25

Ice Thickness Versus Bearing Capacity

for 170 Ton Craft
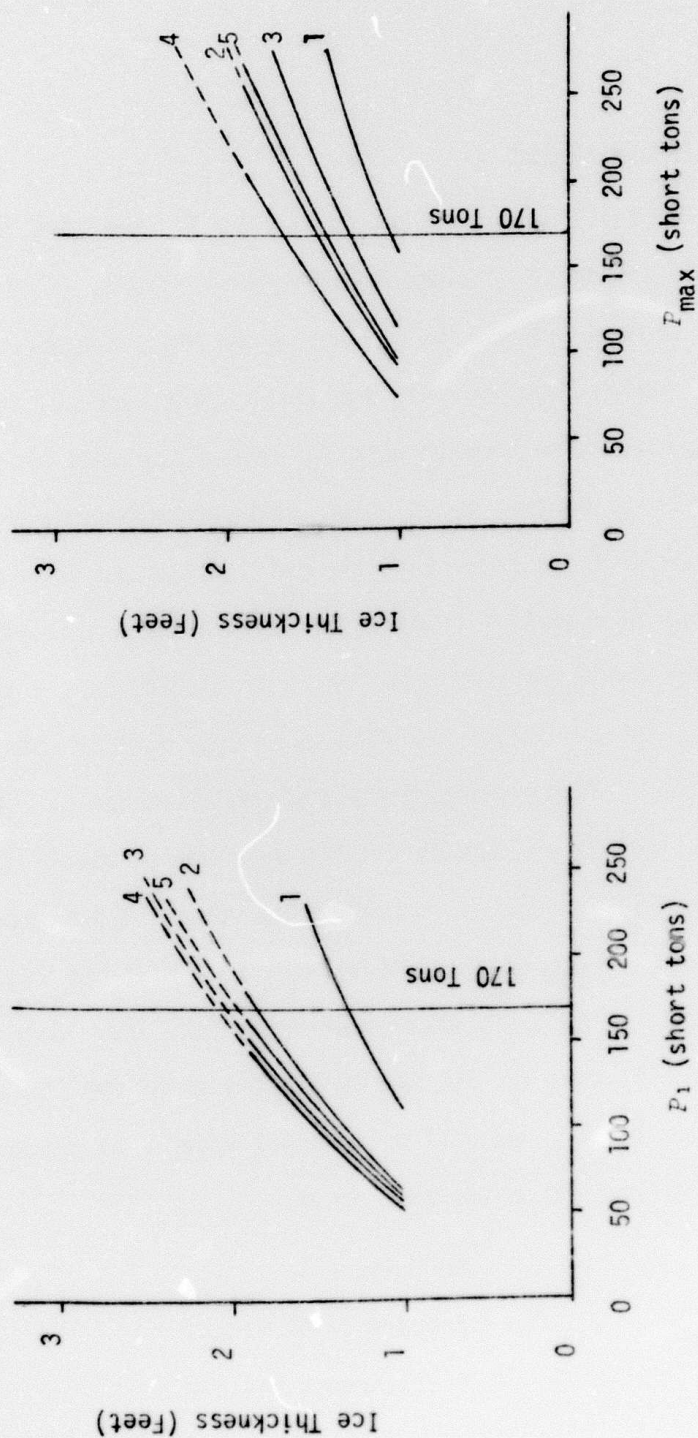
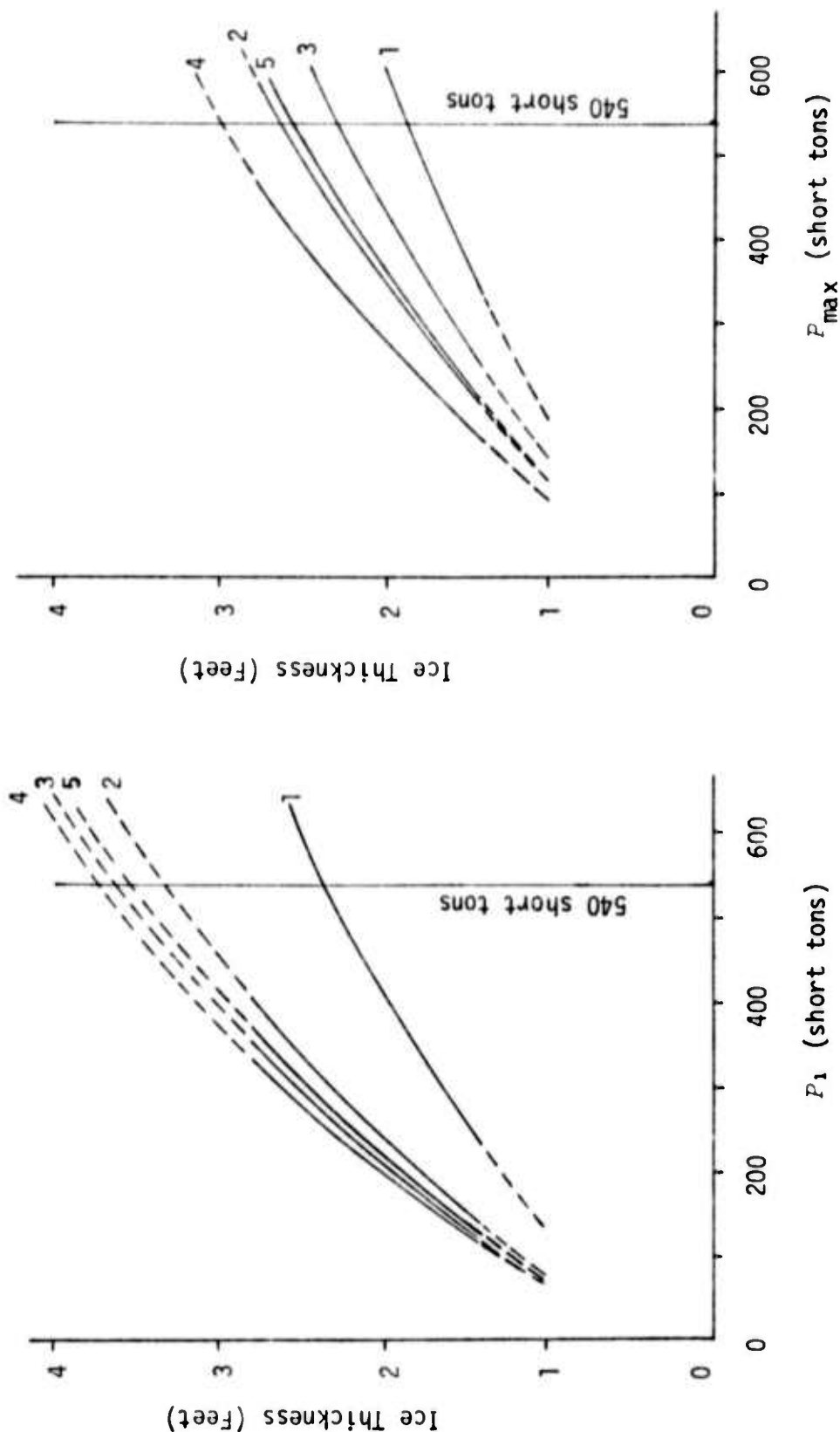$\sigma_f = 70$ psi
$E = 300,000$ psi

———— Range of Data

Models

1. Four Hard Pads
2. Runners
3. Rectangular Inflated Pad
4. Four Inflated Pads
5. Circular Inflated Pad

Figure 26

Ice Thickness Versus Bearing Capacity

for 540 Ton Craft

Models

1. Four Hard Pads
2. Runners
3. Rectangular Inflated Pad
4. Four Inflated Pads
5. Circular Inflated Pad

Figure 27

Ice Thickness Versus Bearing Capacity
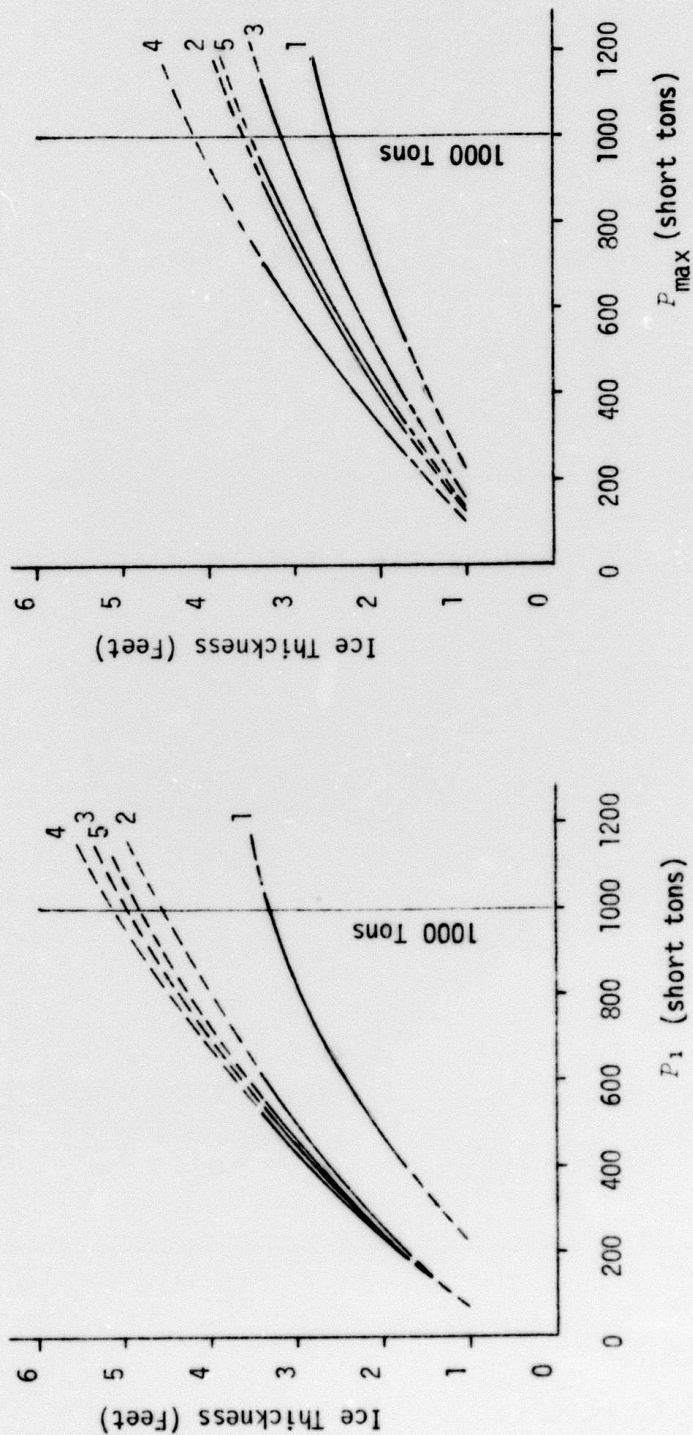
for 1000 Ton Craft

σ_f = 70 psi

E = 300,000 psi

——— Range of Data

Models

1. Four Hard Pads
2. Runners
3. Rectangular Inflated Pad
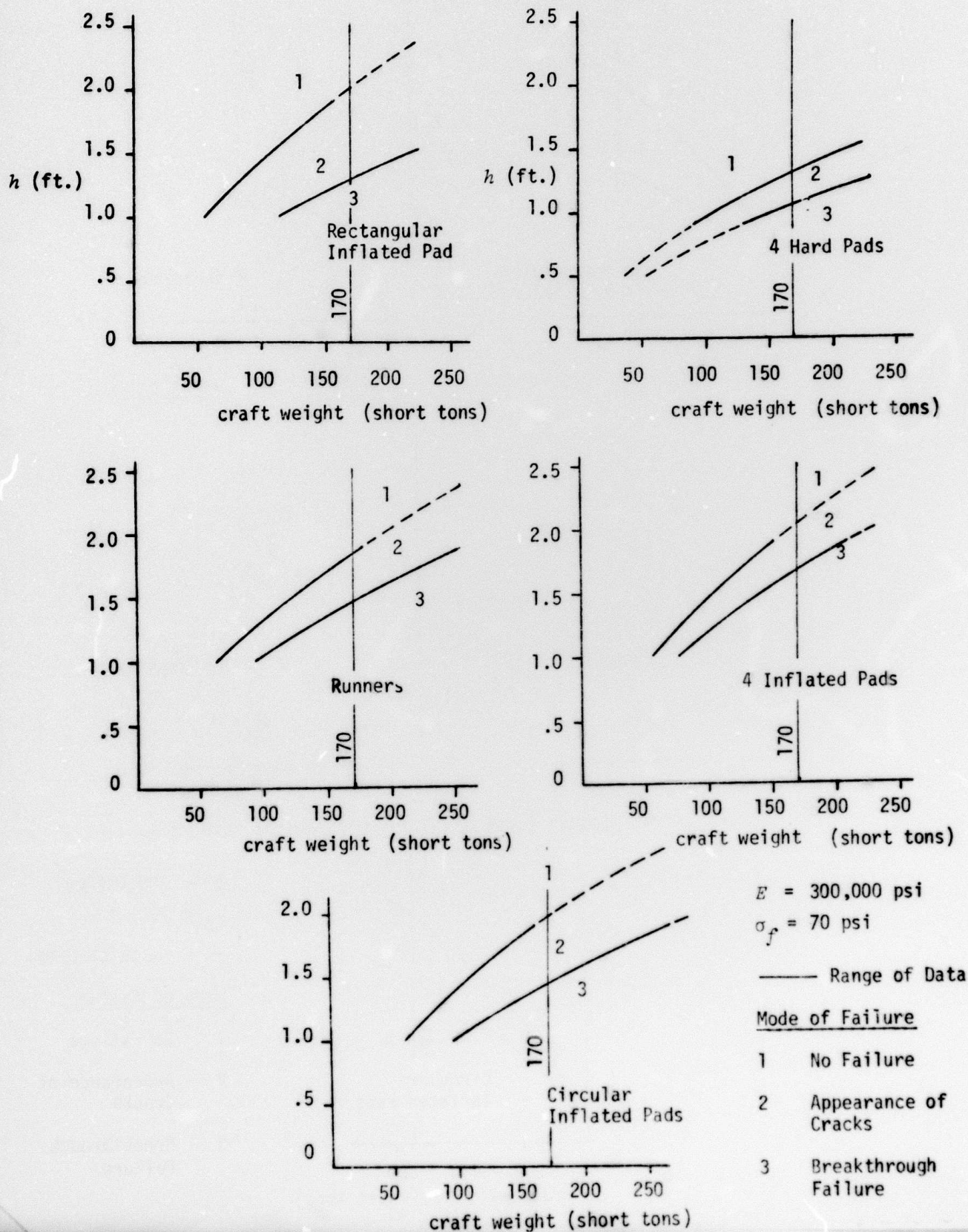4. Four Inflated Pads
5. Circular Inflated Pad

Figure 28

Failure Mode for 170 Ton SEV.

$E = 300,000$ psi
$\sigma_f = 70$ psi

—— Range of Data

Mode of Failure

1   No Failure

2   Appearance of
     Cracks

3   Breakthrough
     Failure

Failure Mode fro 540 Ton SEV.

E = 300,000 psi

σ_f = 70 psi

——— Range of Data

<u>Mode of Failure</u>

1   No Failure

2   Appearance of Cracks

3   Breakthrough Failure

Figure 30

Failure Mode for 1000 Ton SEV.

E = 300,000 psi

σ_f = 70 psi

——— Range of Data

Mode of Failure

1 No Failure

2 Appearance of Cracks

3 Breakthrough Failure
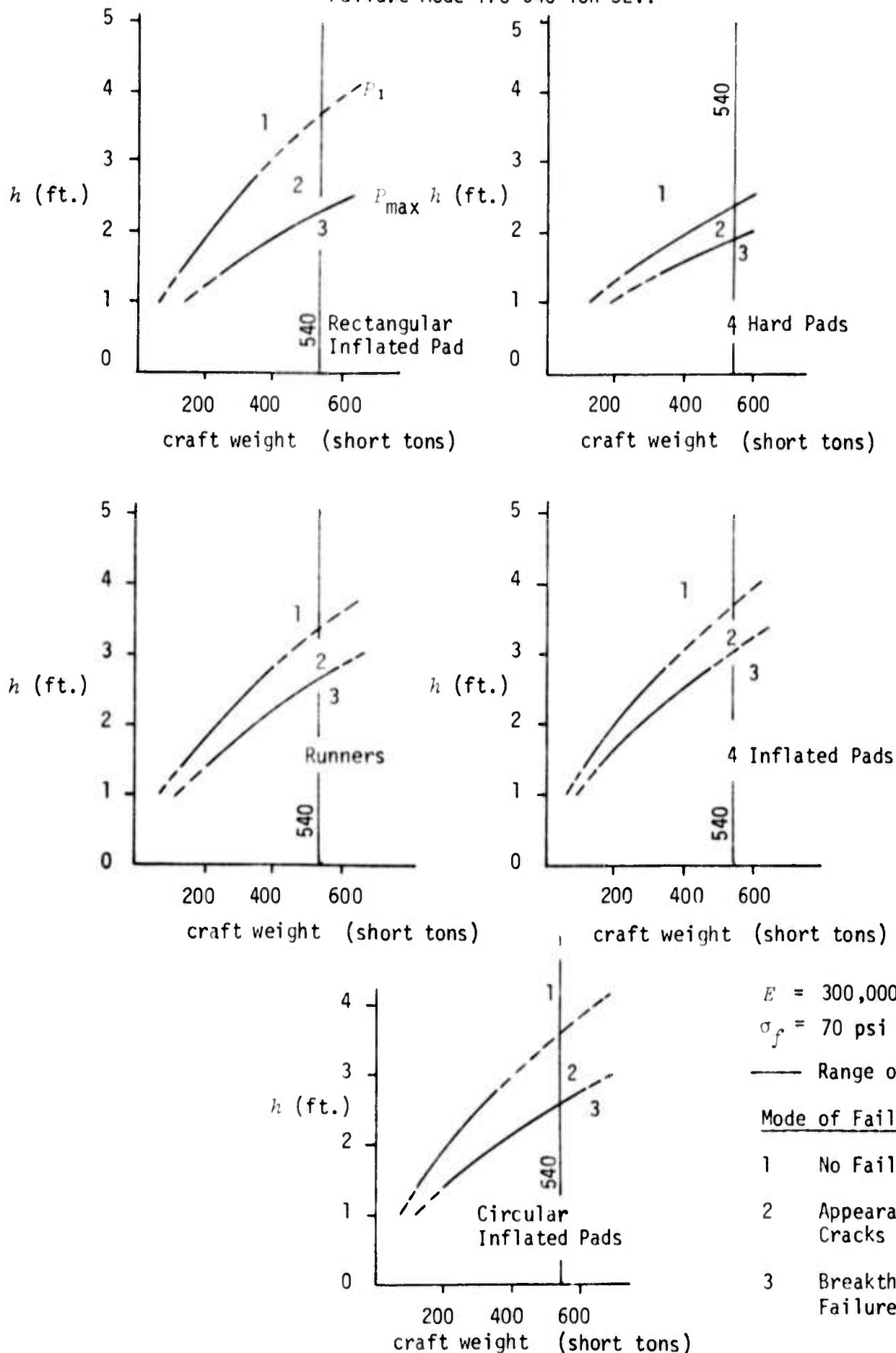
In using these plots in this manner it should be noted that:

(1) The ice thickness of interest is beyond the range of data for some of the models. In formulating the test plan for these tests, it was thought that the non-dimensional bearing capacities ($P_1/\sigma_f h^2$ and $P_{max}/\sigma_f h^2$) would be independent of the load size (L_b/ℓ) since L_b was between 3 to 6 times the ice characteristic length ℓ. If this were true, the range of data would have easily included the ice thicknesses of interest. Also if this were true the bearing capacity, P_1 and P_{max}, would have been predicted higher than what a given thickness of ice could support in reality. Therefore, as a result of these model tests, it was discovered that the bearing capacities are still a function of load size (L_b/ℓ) and that thicker ice is required to support a given craft than was first thought.

(2) From these plots it would first appear that the model with four hard pads would be the best choice since it requires the thinnest ice to support the craft. These pads, however, for the 170 ton craft are only 5 inches high. Because of this, as the craft begins to park and depress the ice sheet, the hull of the craft will come in contact with the ice at the periphery of the flat bottom. The craft is no longer completely off the ice and its hull structure is supporting a portion of the total weight of the craft. The reason why this configuration appears to be the best is because the weight is being distributed over a larger area. If these pads were of the same height as the inflated pads, the failure response would have been similar.

Conclusions and Recommendations

From Figures 28, 29 and 30 presented in the previous section, a summary table (Table 8) can be written for the mode of failure of the ice during parking as a function of ice thickness for different landing pad configurations. In this table, the results for the Four Hard Pads have not been included because of the discussions presented in the previous section. In addition, the results for the Circular Pad were not included because it is not a realistic alternative design. From this table it is interesting to observe there is no tremendous difference between these landing pad configurations. Therefore in practical working terms the 170 ton craft will breakthrough the ice if the ice is less than about 1.5 feet.* On the other hand, the ice will support the craft without cracks forming if the ice is greater than approximately 2 feet.*

A significant reduction in the thickness of ice required to support the craft can be achieved by increasing the area over which the weight is distributed. This is the effect which was seen in the results of the tests with the four hard pads.

It should be emphasized that some of the above stated responses are for ice thicknesses beyond the range of data collected during the

*

σ_f = 70 psi

E = 300,000 psi

model tests as discussed in the previous section. Because of this we recommend that additional tests be conducted in thicker ice in order to extend the range of the test data. By doing this we can gain confidence in the above predictions of the required ice thickness necessary to support the craft.

Table 8

Summary of Parking Test Results

	Mode of Failure		
	No Failure	Appearance of Cracks	Breakthrough Failure
170 ton ASEV			
with Four Inflated Pads	$h > 2.2'$	$1.8' < h < 2.2'$	$h < 1.8'$
with Runners	$h > 1.9'$	$1.5' < h < 1.9'$	$h < 1.5'$
with Rectangular Inflated Pad	$h > 2.1'$	$1.3' < h < 2.1'$	$h < 1.3'$
540 ton ASEV			
with Four Inflated Pads	$h > 3.7'$	$3.0' < h < 3.7'$	$h < 3.0'$
with Runners	$h > 3.3'$	$2.6' < h < 3.3'$	$h < 2.6'$
with Rectangular Inflated Pad	$h > 3.6'$	$2.3' < h < 3.6'$	$h < 2.3'$
1000 ton ASEV			
with Four Inflated Pads	$h > 5.1'$	$4.2' < h < 5.1'$	$h < 4.2'$
with Runners	$h > 4.5'$	$3.6' < h < 4.5'$	$h < 3.6'$
with Rectangular Inflated Pad	$h > 4.9'$	$3.5' < h < 4.9'$	$h < 3.5'$

NOTE: Ice Flexural Strength (σ_f) = 70 psi
Ice Elastic Modulus (E) = 300,000 psi

ARCTEC, Incorporated

V.   REFERENCES

1. Newman, J.N. and Poole, F.A.P., "The Wave Resistance of a Moving Pressure Distribution in a Canal," *Schiffstechnik*, Volume 9, pp. 21-26, 1962.

2. Barratt, M.J., "The Wave Drag of a Hovercraft," *Journal of Fluid Mechanics*, Volume 22, part 1, pp. 39-47, 1965.

3. Doctors, L.J. and Sharma, S.E., "The Wave Resistance of an Air-Cushion Vehicle in Steady and Accelerated Motion," *Journal of Ship Research*, Volume 16, No. 4, pp. 248-260, December 1973.

4. Nevel, D.E., "Moving Loads on a Floating Ice Sheet," U.S. Army Cold Regions Research and Engineering Laboratory, Hanover, N.H., May 1968.

5. Gersten, Alvin, "Performance of an Air Cushion Vehicle with a Peripheral Bag and Finger Skirt in Random Waves," T and F. Report No. 378-H-14, NSRDC, Carderock, Md., March 1971.

6. _____, "Hovercraft Is Being Used as Icebreaker," *Watertown Daily Times*, Watertown, N.Y., April 16, 1974.

APPENDIX A

HOVERCRAFT IS BEING USED AS ICEBREAKER

This article appeared in the *Watertown Daily Times*, Watertown, New York, on April 16, 1974 and is copied with the permission of the *Watertown Daily Times*.

Watertown Daily Times, Watertown, New York
April 16, 1974

Hovercraft Is Being Used as Icebreaker

TORONTO — A hovercraft has been used for a series of ice-breaking tests in Toronto which appear promising, but there still are many experiments to be conducted before a clear-cut case can be made for air cushion vehicle.

The series of ice-breaking tests carried out in Toronto Harbor using hovercraft, may help prove that the development of special icebreaking equipment based on the air cushion principle is economically feasible.

The tests, set up by the Transportation Development Agency of the Ministry of Transport to ascertain the icebreaking capabilities of a hovercraft, were carried out by the ministry's air cushion vehicles section in Toronto's outer Harbor using two air cushion barges.

The barges, one British-built and one constructed in Thornhill, Ont., were not self propelled and were moved about in the harbor area by Toronto Harbor Commission tugs.

"The hovercraft was never designed to go over ice," explained project manager Roger Poitras, "and the fact that it can break ice was really discovered by accident."

Tests were carried out near Yellowknife with an air cushion transporter, a non-self-propelled platform weighing 180 tons fully loaded and it was found capable of breaking ice up to 27 inches thick.

The ice-breaking qualities of the craft were investigated by putting a camera underneath the skirt.

David Dickins, an ice expert with Environmental Canada explains what happened.

"At a slow speed, the air cushion vehicle breaks ice by depressing the water surface immediately beneath the craft below the lower ice surface. As the hovercraft moves forward, the ice breaks under its own weight as the water buoyancy is removed."

Experts have found that in some cases, this air cavity formed between water and ice may extend up to 30 feet ahead of the vehicle and pre-crack the sheet by heaving it up slightly.

The 65-foot Voyageur hovercraft which underwent a series of trials in Toronto Harbor before it was purchased by the Ministry of Transport in 1972, was also evaluated for its ice-breaking capabilities. Loaded to its maximum capacity of 88,000 lbs., and traveling at between four and five miles per hour, the hovercraft was able to break up 10 inch-thick ice. Moving at higher speeds (10-15 m. p. h.) ice was found to be broken in a slightly different manner. The hovercraft creates a large wave of water under the ice about 10 feet behind itself which weakens and cracks the ice. Very good results are obtained by spinning the craft around 180 degrees and meeting the wave head-on.

More tests on this method of ice-breaking were carried out this winter with the Voyageur hovercraft at Parry Sound, Ontario.

Additional tests were also conducted to see whether air cushion vehicles could be used for keeping open small harbours.

"The co-operation of the Toronto Harbor Commissioners was a key factor in selecting Toronto as the site for these tests," said Mr. Poitras.

The two air cushion vehicles used for the tests in Aquatic Park is currently under construction, were the Hover-Jak and the Terracross.

The Hover-Jak, built in Thornhill by the company of the same name, is powered by two 200 h.p. Deutz diesel engines and measures 40 feet by 18 feet. The Terracross, built in Southampton, England, by Air Cushion Equipment, has only one 220 h.p. engine and measures 39 feet by 16 feet.

Both vehicles were able to break ice eight inches thick as they were pushed along by a tug.

"Pushing the vehicle athwartship," Mr. Poitras pointed out, "creates a wider channel of broken ice."

The project manager is enthusiastic about the possibilities for the future.

Preceding page blank